Squashed entanglement: order parameter for topological superconductors

Alfonso Maiellaro, ¹ Antonio Marino, ¹ and Fabrizio Illuminati^{1, 2}

¹ Dipartimento di Ingegneria Industriale, Università di Salerno,
Via Giovanni Paolo II, 132, I-84084 Fisciano (SA), Italy

² INFN, Sezione di Napoli, Gruppo collegato di Salerno, Italy

(Dated: January 28, 2022)

Identifying entanglement-based order parameters characterizing topological systems has remained a major challenge for the physics of quantum matter in the last two decades. Here we show that squashed entanglement between the system edges, defined in terms of the edge-edge quantum conditional mutual information, is the natural order parameter for topological superconductors and for systems with edge modes. In the topological phase, the long-distance edge-edge squashed entanglement is quantized to $\log(2)/2$, half the maximal Bell-state entanglement, and vanishes in the trivial phase. Such topological squashed entanglement exhibits the correct scaling at the quantum phase transition, discriminates between topological order and ordered phases associated to broken symmetries, counts the number of Majorana excitations for systems of increasing geometrical complexity, and is robust against the effects of disorder and local perturbations. In fact, it turns out to be a valid signature of topological order even for systems with weakened bulk-edge correspondence. Squashed entanglement is defined for all quantum states, reducing to the von Neumann entanglement entropy on pure states. As such, it provides a unified framework for the characterization of topological order in any dimension. Squashed entanglement and quantum conditional mutual information are defined in terms of linear combinations of reduced entropies and can thus be probed using currently available experimental setups and techniques.

I. INTRODUCTION

Condensed matter physics is witnessing, among others, two groundbreaking and concurring developments, respectively the application of concepts and methods of quantum information science and the investigation of topological phases of quantum matter.

Via the identification of entanglement boundary laws and their violations, bipartite block entanglement (block von Neumann entropy) has become a central tool for the characterization and the diagnostics of large classes of phenomena in quantum many-body physics [1–5].

At the same time, by featuring perfectly conducting edge modes, patterns of long-distance entanglement and robust ground-state degeneracy without symmetry breaking, three traits that generalize the concept of ordered phase and phase transition beyond the Ginzburg-Landau paradigm, topological states of matter have attracted increasing attention both for their fundamental interest and their potentiality for applications [1–3, 6–9].

In particular, topological superconductors hosting Majorana edge zero modes (MZEMs) [10] have been proposed as the working principle of various disruptive quantum technologies, including fault-tolerant topological quantum computation [11–13].

Topological order in two-dimensional systems is identified and detected by the sub-leading contribution to the bipartite bulk-boundary von Neumann entanglement entropy, the so-called topological entanglement entropy (TEE) [14–16]. This is a great success of entanglement theory applied to the investigation of quantum matter.

Yet, the approach based on block entropies and simple bipartitions is limited and cannot be applied to various important instances, thus showing the need for more gen-

eral and advanced methods of entanglement theory. Indeed, in one dimension at zero temperature, no measure of bipartite entanglement based on simple bipartitions, including the entanglement spectrum, can discriminate topologically ordered phases from those with symmetry-breaking order [17].

Moreover, irrespective of the spatial dimension, being TEE the subleading correction to the leading boundary-law contribution to the ground-state block von Neumann entanglement entropy, it cannot be generalized straightforwardly to finite-temperature and nonequilibrium processes since the von Neumann entropy, when defined on mixed states, includes contributions both from quantum and classical correlations, thus ceasing to be a bona fide measure of entanglement and nonclassicality.

A further limitation of the approach based on the elementary bipartition of the system in two halves is that it is not suitable for the characterization and quantification of the nonlocal correlations that are in place between arbitrary subsystems; in particular, block entanglement entropy provides no information on the physics of edge correlations and cannot characterize and quantify the long-distance entanglement between edge modes. Therefore, going beyond the approach based on simple bipartitions by introducing bipartite entanglement measures defined on multipartitions would allow to identify richer conceptual structures and investigate broader classes of complex physical phenomena.

Thus motivated, in the present work we discuss a multipartition-based measure of bipartite entanglement, the squashed entanglement (SE), previously introduced in the general context of quantum information theory, and we apply it to the study of topological superconductors with model Hamiltonians supporting Majorana

zero energy modes (MZEMs) at the system edges. We show that the long-distance squashed entanglement SE between the edges, that we name topological squashed entanglement (TSE), is the nonvanishing order parameter that 1) characterizes unambiguously the topologically ordered phases of topological superconductors, 2) discriminates topological order from Ginzburg-Landau order associated to spontaneous symmetry breaking and nonvanishing local order parameters, and 3) distinguishes between different types of topologically ordered phases.

As we will show, one can define two basic forms of upper bounds on bipartite SE, respectively in terms of tripartitions and quadripartitions. This general property of SE allows to introduce two forms of TSE, the first one based on edge-bulk-edge tripartitions, the second one based on edge-bulk-bulk-edge quadripartitions. We will then show how the latter identifies unambiguously topological order in the Kitaev chain, discriminates it from standard Ginzburg-Landau order in the Ising chain, is stabilized in the presence of interactions, and is robust against the effects of disorder. Further, we will discuss how the TSE discriminates between different topological phases in models defined on geometries of higher complexity such as two-leg Kitaev ladders. Finally, we will consider models with long-range hopping and consequently suppressed bulk-boundary correspondence, such as the Kitaev tie, and we will show that even in this case the TSE is a good identifier of topological order.

The paper is organized as follows. In Section II we introduce the SE, review its main properties, and introduce the two fundamental forms of upper bounds. In Section III we review the basic models of topological superconductivity in different lattice geometries and define the different forms of TSE corresponding to tripartitions and quadripartitions. In Section IV we discuss in detail the TSE of the 1D Kitaev model for topological superconductivity, compare it to the end-to-end SE in the Ising chain, and discuss the effects of interactions and disorder. In Section V we study the TSE of the two-leg Kitaev ladder and show how it distinguishes between the different topological phases of the model, while in Section VI we carry out the same investigation for the case of the Kitaev tie with long-range hopping and attenuated bulk-boundary correspondence. Finally, in Section VII we discuss our results and further possible applications of SE in the study of quantum matter.

II. SQUASHED ENTANGLEMENT

A. Definition and fundamental properties

We are looking for a measure of bipartite entanglement that has the following properties:

1. It is defined in any spatial dimension, at any temperature, and on all quantum states (pure or mixed).

- It is bipartite but generically defined in terms of non-overlapping, distinguishable multipartitions, and it reduces to the bipartite von Neumann entanglement entropy on pure states of simple bipartitions.
- 3. It is a true, bona fide measure of bipartite entanglement, i.e. a convex entanglement monotone that in addition is also asymptotically continuous, monogamous, and additive on tensor products [18, 19].

In fact, such a measure exists and is the so-called squashed entanglement (SE) [20, 21]. Given a quantum state ρ_{AB} of a bipartite quantum system AB, the SE $E_{sq}(\rho_{AB})$ between subsystems A and B in state ρ_{AB} is defined as:

$$E_{sq}(\rho_{AB}) = \inf_{\rho_{ABC}} \left\{ \frac{1}{2} I(A:B|C) \right\}, \tag{1}$$

where the infimum is taken over all the quantum-state extensions of arbitrary size ρ_{ABC} such that $\rho_{AB} = Tr_C(\rho_{ABC})$, and I(A:B|C) is the quantum conditional mutual information (QCMI) between A and B conditioned by C [22, 23]:

$$I(A:B|C) = S(\rho_{AC}) + S(\rho_{BC}) - S(\rho_{C}) - S(\rho_{ABC}), (2)$$

where $\rho_{AC} = Tr_B(\rho_{ABC})$, $\rho_{BC} = Tr_A(\rho_{ABC})$, $\rho_C = Tr_{AB}(\rho_{ABC})$, and $S(\rho)$ denotes the von Neumann entropy of a given quantum state ρ [19].

SE owes its name by the construction Eqs. 1–2 that "squashes" out the classical correlations to leave only the quantum contributions to the mutual information between parties A and B conditioned by party C (that in informatic terms can be seen as the "conditioning environment"). SE is a lower bound on the entanglement of formation and an upper bound on the distillable secret key or distillable entanglement of a quantum state or a quantum channel [21, 24], and reduces to the von Neumann entanglement entropy on pure states of a bipartite system AB. Indeed, if ρ_{AB} is pure, then $\rho_{ABC} = \rho_{AB} \otimes \rho_C$, and thus $E_{sq}(\rho_{AB}) = [S(\rho_A) + S(\rho_B)]/2 = S(\rho_A) = S(\rho_B)$.

SE is unique in that it is the only known entanglement quantifier that enjoys all the desirable axiomatic properties required for a bona fide measure of entanglement [19]. SE is a full entanglement monotone, i.e. non increasing under local operations and classical communication (LOCC), and convex [21]: $E_{sq}(\lambda \rho + (1 - \lambda)\sigma) \leq \lambda E_{sq}(\rho) + (1 - \lambda)E_{sq}(\sigma)$, with $\lambda \in [0, 1]$. Moreover, SE enjoys important additional properties that promote it to a full entanglement measure.

First of all, SE is additive on tensor products [21]: $E_{sq}(\rho \otimes \sigma) = E_{sq}(\rho) + E_{sq}(\sigma)$. SE is also continuous [25]: if two sequences of states ρ_m and σ_m converge in trace norm: $\lim_{m\to\infty}\|\rho_m-\sigma_m\|_1=0$, then $\lim_{m\to\infty}E_{sq}(\rho_m)-E_{sq}(\sigma_m)=0$. Furthermore, SE is faithful, that is, $E_{sq}(\rho_{AB})\geq 0$, and $E_{sq}(\rho_{AB})=0$ if and only if ρ_{AB} is separable [26].

Finally, SE is monogamous [27]: given three parties A, B, and C, one has: $E_{sq}(\rho_{A|BC}) \geq E_{sq}(\rho_{AB}) + E_{sq}(\rho_{AC})$, that is, the bipartite SE cannot be freely shared among multiple parties; in particular, if A is maximally entangled with B, then it cannot be entangled with C. This property has important consequences on the SE between edge modes that we will study later on in this work.

SE is an entanglement measure with very important operational meaning. In quantum communication theory it is defined in terms of the communication cost in the distribution of quantum states among multiple parties [28] and it is a tight upper bound on the length of a secret key shared by two parties holding many copies of a quantum state [24, 29]. Moreover, it allows for multipartite extensions with operational meaning [30]. Finally, SE plays a fundamental role in channel theory, as the SE of a quantum channel is the optimal upper bound on the quantum communication capacity of any channel assisted by unlimited classical communication [31].

Although computing SE is NP-complete [32], it has been calculated analytically for some nontrivial classes of states [33, 34]; moreover, it enjoys a set of very useful lower bounds in terms of the reduced von Neumann entropies, the relative entropy of entanglement and the relative 2-Rényi entropy [29, 35–37].

B. From bipartitions and two blocks to multipartitions and any pair of subsystems

Given a physical system G in a pure state $\rho_G = |G\rangle\langle G|$, typically a ground state in condensed matter physics and quantum statistical mechanics or a vacuum state in quantum field theory, one typically focuses on simple bipartitions G = AB of system G in two blocks A and B, and considers then the pure–state bipartite entanglement between the two blocks as quantified by the von Neumann block entanglement entropy $S(\rho_A) = S(\rho_B)$ of the reduced local states $\rho_A = Tr_B\rho_G$ or, equivalently, $\rho_B = Tr_A\rho_G$.

Squashed entanglement greatly extends this picture to include all possible different forms of bipartite entanglement. To set the stage, consider a quantum system G in an arbitrary state ρ_G . Next, consider partitioning the global system G in any two subsystems A and B plus a reminder C: G = ABC. When C is the empty set and ρ_G is a pure state, we recover the standard two–block bipartition and SE reduces to the von Neumann block entanglement entropy.

We now wish to determine the SE $E_{sq}(\rho_{AB})$ existing between subsystem A and subsystem B in the reduced state ρ_{AB} . The first important observation in order is that there are always two, and only two, equivalent ways to obtain the same reduced state ρ_{AB} from the global state ρ_G that however give rise to two, and only two, different expressions for the QCMI of Eq. 2 prior to the extremization procedure in Eq. 1 that defines the SE. These two different expressions of the QCMI define two fundamental upper bounds on the true SE that may in principle be different. The two expressions obviously give rise to the same unique SE once extremization is performed in Eq. 1.

Indeed, besides the immediate tripartite form $\rho_G = \rho_{ABC}$ such that $\rho_{AB} = Tr_C(\rho_{ABC})$, one can consider a further bipartite splitting of the reminder: $C = C_1C_2$ and obtain the corresponding quadripartite form $\rho_G = \rho_{ABC} = \rho_{ABC_1C_2}$ such that $\rho_{AB} = Tr_{C_1}(\rho_{ABC_1})$ (or, equivalently, $\rho_{AB} = Tr_{C_2}(\rho_{ABC_2})$), where in turn $\rho_{ABC_1} = Tr_{C_2}(\rho_{ABC_1C_2})$ (or, equivalently, $\rho_{ABC_2} = Tr_{C_1}(\rho_{ABC_1C_2})$). We can thus introduce in Eq. 2 two different expressions for the QCMI: $I_{(3)}(A:B|C)$ and $I_{(4)}(A:B|C_1)$ (or, equivalently, $I_{(4)}(A:B|C_2)$) based, respectively, on the tripartition ABC and on the quadripartition ABC_1C_2 :

$$I_{(3)} = S(\rho_{AC}) + S(\rho_{BC}) - S(\rho_{ABC}) - S(\rho_C), \qquad (3)$$

$$I_{(4)} = S(\rho_{AC_1}) + S(\rho_{BC_1}) - S(\rho_{ABC_1}) - S(\rho_{C_1}), (4)$$

where $S(\rho_{ABC}) = 0$ if $\rho_{ABC} = \rho_G$ is pure.

The QCMIs $I_{(3)}$ and $I_{(4)}$ define the two natural upper bounds, respectively in terms of tripartitions and quadripartitions, to the SE $E_{sq}(\rho_{AB})$. It is immediate to verify that any further splitting of the reminder C in multipartitions of higher order $C = C_1 C_2 C_3 \dots C_n$ is redundant and trivially reproduces the QCMI $I_{(4)}$. Taking into account the subadditivity properties of the von Neumann entropy and the triangle inequality, one has $I_{(3)} \geq I_{(4)}$, so that the chain of inequalities reads

$$I_{(3)}(A:B|C) \ge I_{(4)}(A:B|C_1) \ge E_{sq}(\rho_{AB}).$$
 (5)

The two fundamental constructions, respectively via the tripartition ABC and the quadripartition ABC_1C_2 , are summarized in panels (a) and (b) in Fig. 1.

The exact $A{-}B$ bipartite SE in state ρ_{AB} is obtained by computing the infimum of the two expressions Eqs. 3–4 over all extensions of unbounded dimension ρ_{ABC} and ρ_{ABC_1} , respectively. This is in general an exceedingly hard task; on the other hand, the true SE is readily obtained whenever there are lower bounds available that coincide with some upper bounds, for instance like the ones provided by Eqs. 3–4.

Summarizing what has been discussed so far, we have shown how by resorting to the QCMI and the SE one moves from the elementary paradigm of bipartite pure—state block entanglement entropy defined over minimal, irreducible bipartitions of the global system to a general framework of bipartite entanglement between any two subsystems defined over arbitrary multipartitions of the global system. Moreover, we have introduced two classes of upper bounds to the exact SE defined over tripartitions and quadripartitions of the global system. The transition from bipartitions to multipartitions and from block entanglement to SE of generic subsystems is

pictured in panels (c) and (d) of Fig. 1, where we illustrate schematically how such transition allows in principle to discriminate systems with broken symmetries and short-ranged entanglement from systems with a different type of global order and long-distance boundary entanglement. In the next sections we investigate in detail some significant consequences of this paradigm shift in the study of topological quantum matter.

III. SQUASHED ENTANGLEMENT AND TOPOLOGICAL SUPERCONDUCTORS

A. The quest for order parameters

The archetypal model of topological p-wave superconductivity supporting Majorana edge zero modes (MZEMs) is the Kitaev Hamiltonian of spinless fermions on a 1D lattice [38]. Proposals for realistic implementations of the Kitaev chain consider heterostructures made of semiconducting nanowires coupled to s-wave superconducting substrates [39–42].

Experimental evidence of MZEMs localized at the system edges has been obtained in the study of the tunnel conductance of an InAs nanowire proximized by an swave superconductor [43] and in the scanning tunneling microscopy of iron-atom chains deposited on lead substrates [44].

The one-dimensional Kitaev model can be generalized to geometries of significantly increasing complexity, e.g. via Kitaev ladders and ties, to describe coupled superconducting nanowires with a phase diagram hosting a rich variety of different topological phases [45–50].

In view of its conceptual significance and potential realizability in realistic systems of condensed matter physics, the Kitaev model has become a central paradigm in the study of topologically ordered phases of matter hosting MZEMs and, more generically, edge modes and edge states.

The problem of identifying unambiguous signatures of topologically ordered phases, such as topological invariants and/or nonlocal order parameters, has turned out to be a highly nontrivial task addressed in a number of different approaches. One can look to momentum-space properties [51], when, after imposing periodic boundary conditions, the translational invariance is restored. This meaningful relation between the edges and the bulk of a system is also known as bulk-edge correspondence [51] and leads to the definitions of geometric indices Q which signal the presence and the number of topological zero-energy states of matter.

Unfortunately, for disordered systems or, in general, when translational invariance cannot be restored, or also in the presence of interactions, the topological invariants Q are no longer valid signatures and indicators of topological phase transitions and topologically ordered phases [52–55].

In a more fundamental approach one tries then to

identify topological invariants based on the entanglement properties of the system, such as the entanglement spectrum [17, 56, 57] or the Rényi entropies of disconnected and partially overlapping partitions [58].

Indeed, the entanglement spectrum becomes two-fold degenerate when a quantum system undergoes a topological phase transition [59–61]; however, this is not a discriminating signature of topological order: exactly the same degeneration is featured by any system with the same Hamiltonian symmetries that can support symmetry-breaking order [17, 62]. As a consequence, block entanglement based on simple bipartitions and two blocks does not provide the information necessary to identify and discriminate unambiguously topological order associated to edge modes and edge states.

Suitable combinations of Rényi entropies of disconnected and partially overlapping multipartitions actually allow to define quantized topological invariants able to characterize topologically ordered phases in one-dimensional topological superconductors [58]. This is a significant step forward. Unfortunately, these invariants are not entanglement monotones between distinguishable subsystems, let alone entanglement measures, and thus are devoid of a clear physical meaning in terms of nonlocal quantum correlations.

Even leaving aside their lack of conceptual significance, it is difficult from a purely pragmatic point of view to understand how to develop such invariants systematically for the characterization of different types of topologically ordered phases or to extend them to general situations such as finite temperature and/or complex geometries and higher dimensions.

In the present work, we discuss SE in the context of topological quantum matter featuring edge modes and edge states. We show that the edge-to-edge, long-distance bipartite SE is an order parameter, properly quantized, featuring the correct scaling behavior at the critical point, characterizing the ordered phases of topological superconductors in various geometries, and discriminating them unambiguously from other classes of ordered phases of matter.

Shifting focus from block entanglement entropy to SE between subsystems finds a basic physical motivation by observing that systems with topological order display bulk band gaps like those of ordinary insulators and conducting surface states that are topologically protected by some symmetries. This naturally prompts to look for nonlocal correlations between subsystems (e.g. the system edges) rather than the block entanglement between two halves of the same system. In turn, this implies replacing bipartitions with multipartitions, and resorting to SE as the prospective quantity able to:

- Quantify the prima facie bipartite edge-edge, longdistance entanglement in the presence of edge modes.
- Discriminate unambiguously topological order from symmetry-breaking order and distinguish between

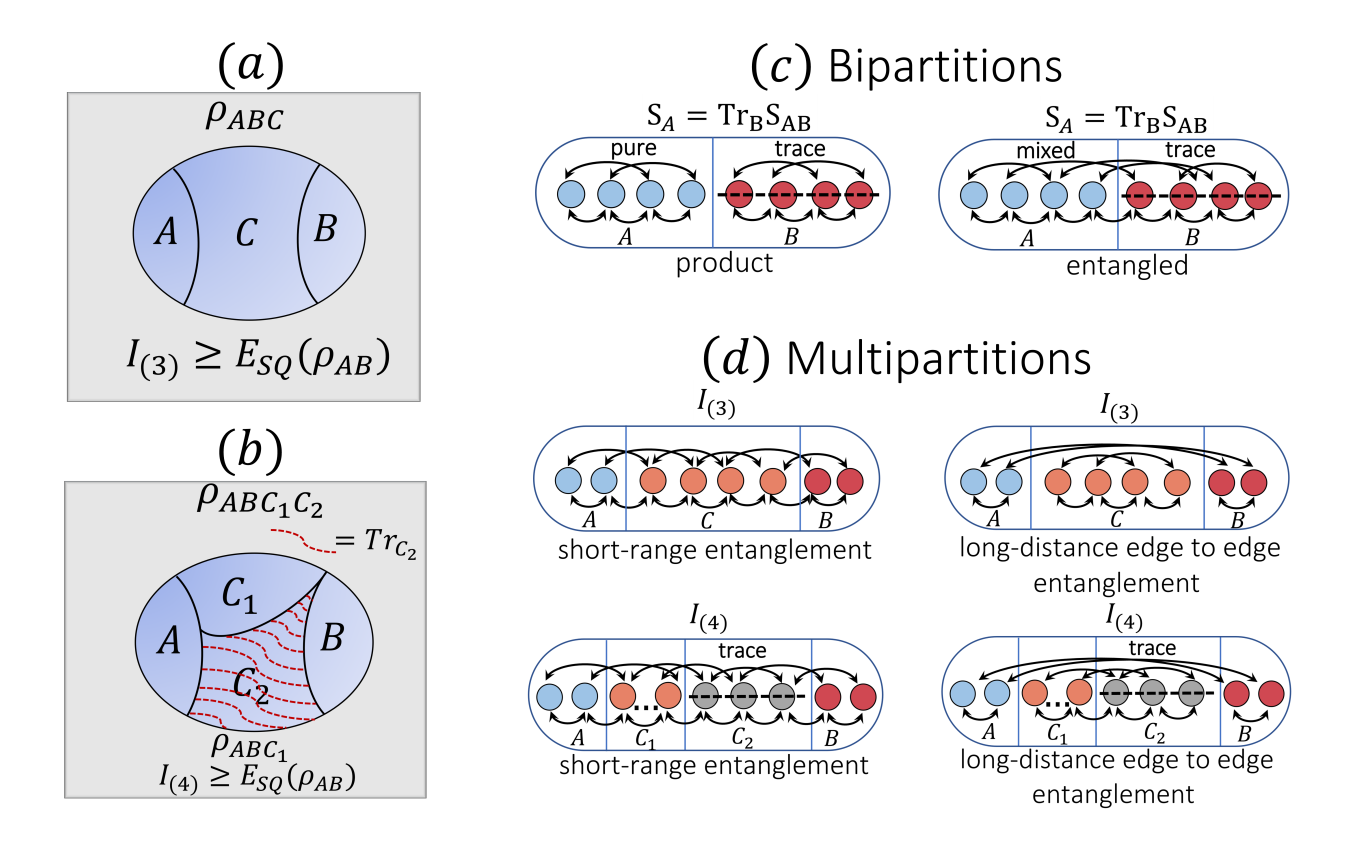


FIG. 1. Panels (a) and (b): Construction pattern of the two upper bounds, the QCMIs $I_{(3)}(A:B|C)$ and $I_{(4)}(A:B|C_1)$, on the true SE between two arbitrary subsystems A and B of a given quantum system in an arbitrary global state, pure or mixed. Panel (c): A system in a globally pure state is partitioned in two subsystems (blocks); after tracing over the degrees of freedom of one of the blocks, the von Neumann entropy of the reduced state defines the block entanglement entropy quantifying the bipartite entanglement across the blocks separation boundary. Panel (d): From block entanglement to SE between subsystems. We illustrate the case of the long-distance SE and QCMIs $I_{(3)}(A:B|C)$ and $I_{(4)}(A:B|C_1)$ between the system edges A and B separated by the bulk $C = C_1C_2$. This is the case of interest, e.g., in the study of topological order in quantum matter. The double-headed arrows represent pictorially the spatial ranges of the different quantum correlation patterns.

different classes of topologically ordered phases.

In the following we will consider systems hosting MZEMs and for such systems we will investigate the two bipartite edge-to-edge QCMIs, $I_{(3)}(A:B|C)$ and $I_{(4)}(A:B|C_1)$ that realize two upper bounds on the true SE $E_{sq}(\rho_{AB})$ between edge A and edge B. In particular, we will show that the QCMI $I_{(4)}$ discriminates the one-dimensional Kitaev model featuring edge modes and long-distance entanglement between the edges from the Ising chain, its symmetry-breaking counterpart featuring no edge modes and a short-distance entanglement structure.

For the Kitaev chain we will show that $I_{(4)}$ satisfies all the requirements for a genuine topological order parameter, including: quantization as topological invariant at the exact topological ground-state degeneracy point and throughout the topologically ordered phase, scaling with the system size at the phase transition point, and robustness against localized disorder and imperfections.

Moreover, for the Kitaev chain the topological invariant in fact coincides with a lower bound to the SE, and

therefore the QCMI $I_{(4)}$ indeed coincides with the edge SE E_{sq} at the exact topological degeneracy point and throughout the entire topologically ordered phase. The transition from simple bipartitions and block entanglement entropy to multipartitions and edge to edge long-distance entanglement is illustrated pictorially in panels (c) and (d) of Fig. 1.

We will then generalize the method to consider models of topological superconductors defined on geometries of higher complexity, the Kitaev ladder [49] and the Kitaev tie [50]. The Kitaev ladder model is obtained by coupling two Kitaev chains by means of transverse hopping and pairing terms.

The Kitaev chain and the Kitaev ladder belong to the two different topological classes D and BDI which are characterized by two different topological bulk invariants, respectively the Pfaffian invariant [63] and the winding number [49]. In the case of the Kitaev tie, the long-range hopping term added to the Hamiltonian of the Kitaev chain define a knotted—ring geometry which can be rearranged in the form of a tie. The model is then the

simplest realization of geometric frustration with no associated bulk [64].

For all three models SE identifies and characterizes the different topological behaviors of the systems, well characterized by the band topology for the Kitaev chain and the Kitaev ladder and by the Majorana polarization and topological transfer matrix for the Kitaev tie [64]. We will show that $I_{(4)}$ identifies the topological phase transitions in the Kitaev ladder and distinguishes between the different topologically ordered phases of the model corresponding to different numbers of Majorana excitations.

Remarkably, in the case of the Kitaev tie, a system which lacks a clearly identifiable bulk, the SE is still very efficient in characterizing the topological phases of the model even if, as expected, perfect quantization is partially blurred due to the less pronounced physical bulk-boundary separation.

B. Topological squashed entanglement

For the model systems defined in the following we consider tripartitions and quadripartitions as sketched in Fig. 1 and we proceed to compute the upper bounds $I_{(3)}(A:B|C)$ and $I_{(4)}(A:B|C_1)$ on the SE $E_{sq}(\rho_{AB})$ between the edges A and B given a bulk $C = C_1C_2$.

In a condensed matter setting, the two QCMIs are defined in terms of the many body ground state, i.e. they are the quantum mutual information of the edges A and B conditioned, respectively, on the existence of the total bulk C and the partial bulk C_1 . When going to sufficiently large system sizes such that the edges are far from each other and decoupled from the bulk, a non-vanishing $E_{sq}(\rho_{AB})$ establishes the existence of a topological squashed entanglement (TSE), i.e. a nontrivial long-distance quantum correlation between the edges.

Although the physical mechanisms are rather different, the edge-edge fermionic TSE is reminiscent of other forms of long-distance entanglement (LDE) that are established by entanglement monogamy between the end points of dimerized and quasi-dimerized spin chains with alternate patterns of strong and weak nearest-neighbor couplings or patterns of competing finite-range interactions [65–67]. In turn, the latter can be seen as particular instances of more general patterns of modular entanglement [68] and surface entanglement on networks [69].

In panels (a)–(c) of Fig. 2 we provide a sketch of the three model geometries considered (Kitaev chain, Kitaev ladder, Kitaev tie), while in panels (d) and (e) we draw a synthetic scheme of how the multipartitions reported in Fig. 1 are applied to these three explicit cases.

As detailed in the next sections, both the Kitaev ladder and the Kitaev tie can be obtained, respectively, from two coupled Kitaev chains and by adding to the Hamiltonian of a single chain a symmetric long-range hopping that couples a single lattice site at position d with its symmetric counterpart at position L-d+1. In panels (d) and (e) of Fig. 2 we provide a schematics of the two

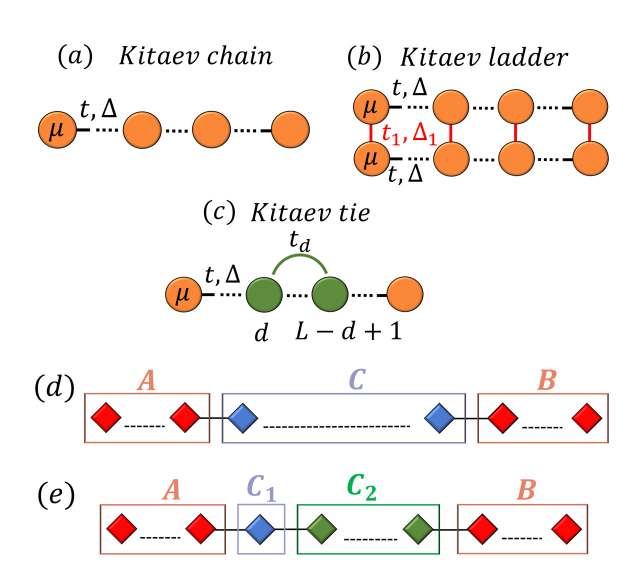


FIG. 2. Schematic of a Kitaev chain (a), a two-leg Kitaev ladder (b) and a Kitaev tie (c). The Kitaev ladder is obtained coupling two Kitaev chains by superconducting and hopping terms. For a Kitaev chain of length L, the Kitaev tie is obtained by adding a long-range hopping term coupling a site at position d with the symmetric one at the position L-d+1. The basic tripartition and quadripartition are reported, respectively, in panels (d) and (e). In both panels the edges are denoted by A and B (red color); in panel (d) the total bulk $C = C_1C_2$ is reported in blue; in panel (e) the bulk portions C_1 and C_2 are reported in blue and in green, respectively. The diamonds are generic and can correspond to a single fermionic site when referred to a chain or a tie and to two fermionic sites when referred to a ladder. In the quadripartition, when not otherwise specified, the length L_{C_1} of the bulk portion C_1 is fixed at $L_{C_1} = 1$.

basic multipartitions for the model systems considered.

In the following, the lengths of the various subsystems will be denoted by L_{α} , with $\alpha=A,\ B,\ C,\ C_1,\ C_2$. Throughout, the lengths of the two edges are assumed to coincide, $L_A=L_B$. Denoting by L the chain length, when not otherwise specified we will set $L_A=L_B=L_e$, with $L_e=L/3$. The latter choice allows to take into account the exponential bulk–edge decoupling behavior as a function of the system size that is typical of topological modes.

Moreover, as explained later on (see Fig. 5, panel (a)), our results will be independent of the relative size of the two sub-bulks, so that without loss of generality we will take $L_{C_1} = 1$ throughout, as reported in panel (e) of Fig. 2.

A crucial step in order to compute the TSE consists in diagonalizing the reduced density matrices of the various subsystems, once the many body ground state density matrix $\rho = |\Psi\rangle_{GG}\langle\Psi|$ is assigned.

When interactions are neglected, the Kitaev-type Hamiltonians are quadratic in the fermionic degrees of freedoms and can be diagonalized by a Bogoliubov transformation. In this case, an appropriate approach to compute the von Neumann entropies of the subsystems has

been introduced by Peschel [70].

The Bogoliubov transformation ensures a direct access to fermionic correlations on the many body ground state $|\Psi\rangle_G$ and the reduced density matrix of a given subsystem α can be recast in the form of a thermal density matrix, $\rho_{\alpha} = (1/Z)e^{-\mathcal{H}_{\alpha}}$, where $\mathcal{H}_{\alpha} = \sum_{l=1}^{L_{\alpha}} \epsilon_l f_l^{\dagger} f_l$ is the effective entanglement Hamiltonian of the reduced system [71–74], and the constant factor Z (the "partition function") ensures the correct normalization $Tr(\rho_{\alpha}) = 1$.

Given the lattice fermionic creation and annihilation operators $\{c_i, c_i^{\dagger}\}$, the spectrum of the entanglement Hamiltonian can be evaluated numerically by solving the eigenvalue problem:

$$(2T - 1 - 2D)(2T - 1 + 2D)\phi_l = \tanh^2\left(\frac{\epsilon_l}{2}\right)\phi_l$$
, (6)

where $T_{ij} = \langle \Psi | c_i^{\dagger} c_j | \Psi \rangle$ and $D_{ij} = \langle \Psi | c_i^{\dagger} c_j^{\dagger} | \Psi \rangle$ are the matrix elements of the fermionic two-point correlations in a quantum state $|\Psi\rangle$ (for instance, the ground state $|\Psi\rangle_G$), and 1 is the identity matrix. The index l runs over all the lattice sites belonging to subsystem α .

Due to the form of ρ_{α} , the von Neumann entropy of the reduced state $S(\rho_{\alpha})$ can be obtained in terms of the eigenvalues of entanglement Hamiltonian:

$$S(\rho_{\alpha}) = \sum_{l} \ln(1 + e^{-\epsilon_{l}}) + \sum_{l} \frac{\epsilon_{l}}{e^{\epsilon_{l}} + 1}.$$
 (7)

The Peschel algorithm for free fermionic systems reduces the computational efforts and allows to access the entanglement properties for systems of very large sizes.

When interactions are included in the models, the mapping to the effective entanglement Hamiltonian and the Gaussian thermal structure of the reduced density matrix are no longer applicable and one must resort to numerical techniques, e.g. the density matrix renormalization group (DMRG) method, particularly well suited to treat one-dimensional systems [75–77].

Complementary to numerical methods, one can resort to direct numerical matrix diagonalization in the parameter region that allows for exact analytic expressions of the state vectors, such as along the exact factorization lines of interacting spin models and Kitaev-type fermionic systems [78–81], as we will discuss in the following.

IV. TOPOLOGICAL SQUASHED ENTANGLEMENT OF THE KITAEV CHAIN

A. The order parameter

Here and in the following we investigate the paradigmatic case of the fermionic Kitaev chain [38], considering first the non-interacting model:

$$H_K = \sum_{j=1}^{L} -\mu c_j^{\dagger} c_j + \sum_{j=1}^{L-1} (\Delta c_{j+1}^{\dagger} c_j^{\dagger} - t c_j^{\dagger} c_{j+1} + h.c.).$$
 (8)

The Hamiltonian H_K in Eq. 8 describes a system of spinless fermions confined to a one dimensional lattice of length L with on site creation and annihilation operators c_j^{\dagger} , c_j $(j=1,\ldots,L)$, subject to a p-wave superconducting coupling. The coefficients Δ , t and μ are respectively the strength of the superconducting pairing, the nearest-neighbor hopping amplitude and the on-site energy offset.

This model features a topological phase for $\mu < 2t$ and $\Delta \neq 0$ with two robust Majorana zero-energy modes localized at the two edges. The energy E_M of such MZEMs scales exponentially to zero with the system's size and is expected to vanish asymptotically in the thermodynamic limit.

In the limit of small on site energy offset (chemical potential), precisely at the analytically solvable point $\mu=0$ and $t=\Delta$, the model features exact topological two-fold ground state degeneracy and two MZEMs with exactly $E_M=0$, independently of the chain length. The remaining non-topological modes of the spectrum are gapped and form a band. In the opposite regime of large on site energy offset $\mu>2t$ the Kitaev wire is a band insulator.

By construction the Hamiltonian satisfies the particle-hole symmetry and belongs to the class \mathcal{D} of the ten-fold classification [82], with topological invariant given by the Pfaffian invariant [63].

For the non-interacting Kitaev chain, we have computed the two QCMIs $I_{(3)}$ and $I_{(4)}$ and verified that $I_{(3)} = I_{(4)}$ throughout the entire phase diagram, so that in the reminder of the present subsection we will focus only on $I_{(4)}$. The physical origin of the two QCMIs' equality in the topological case will become clear in the following.

In panel (a) of Fig. 3 we report the phase diagram obtained by means of the ratio between the QCMI $I_{(4)}$ and the constant quantity $E_{sq}^0 = \log(2)/2$. One finds that throughout the entire topological phase the ratio $I_{(4)}/E_{sq}^0 = 1$ so that $I_{(4)}$ is quantized exactly at the value $I_{(4)} = E_{sq}^0 = \log(2)/2$. Moreover, one has that $I_{(4)} = 0$ throughout the entire trivial phase.

Finite size effects are clearly visible near the phase transition line at $\mu=2t$, as also shown in panel (b) of Fig. 3, where the ratio $I_{(4)}/E_{sq}^0$ is plotted as a function of the length L of the chain for $t=\Delta=1$ and three different values of the chemical potential μ , respectively close to the exact topological point, in the topological phase close to the critical point, and well into the trivial phase.

In particular, $I_{(4)}$ scales exponentially to the quantized value E^0_{sq} inside the topological phase (red curve) and it coincides with E^0_{sq} independently of the size of the chain for values of μ sufficiently close to the analytic point (blue curve). The QCMI identically vanishes at any value of μ in the trivial phase (green curve).

Finally, in panel (c) of Fig. 3 we report the behavior of the QCMI as a function of μ for different values of the length of the chain L, showing the correct approach to quantization inside the topological phase and the correct scaling behavior approaching the critical point. These results show that the QCMI $I_{(4)}$ detects and characterizes

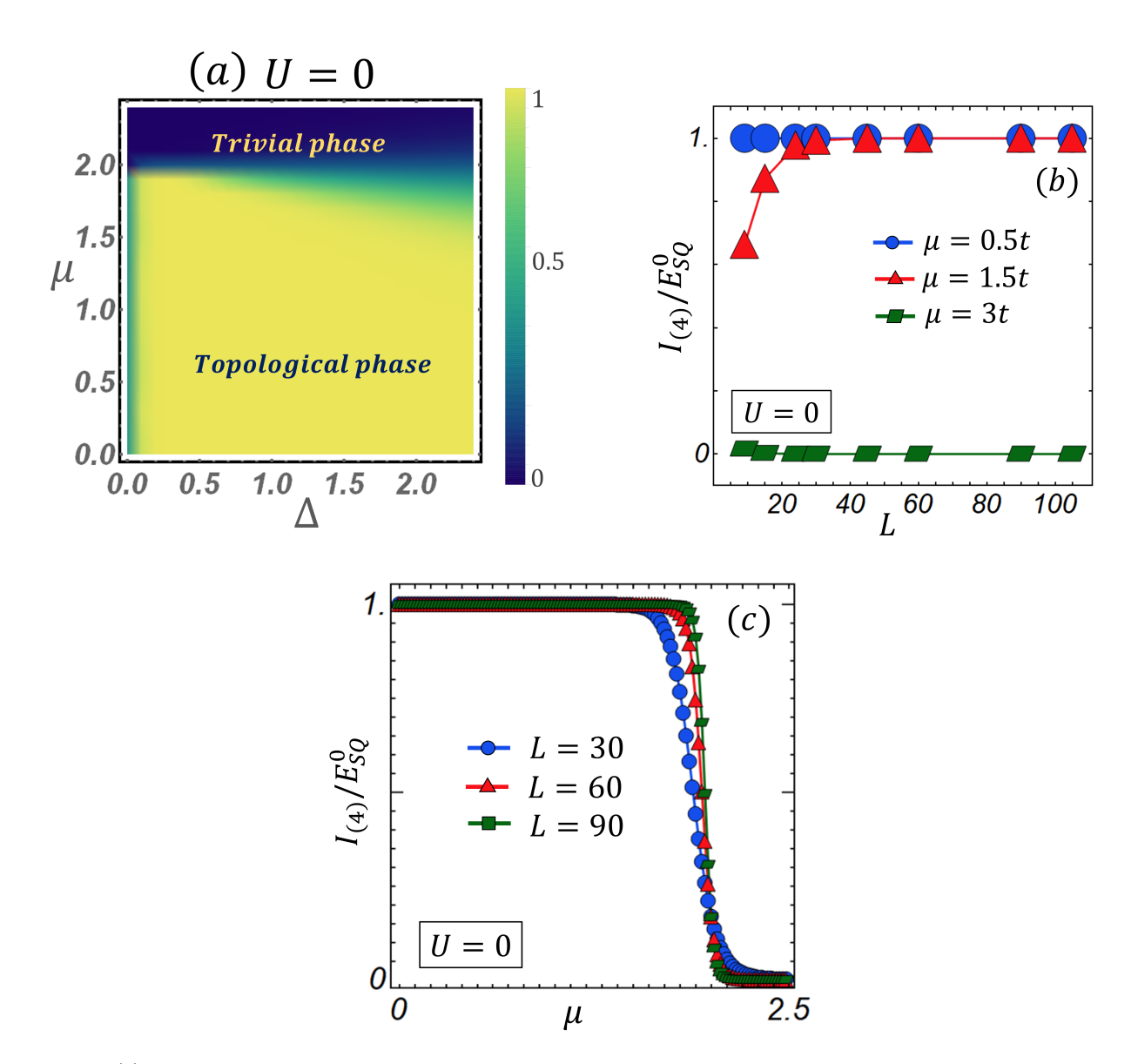


FIG. 3. Panel (a): Phase diagram of the non-interacting Kitaev chain as measured by the two-dimensional contour plot of the ratio between the QCMI $I_{(4)}$ and the TSE $E_{sq}^0 = \log(2)/2$ on the Δ - μ plane with a grid of 25 × 25 points, reference hopping amplitude t=1, chain length L=60, and edge length $L_e=L/3$. Panel (b): Scaling-size effects on $I_{(4)}/E_{sq}^0$ as a function of L=1 for different values of the chemical potential μ . Panel (c): Scaling of $I_{(4)}/E_{sq}^0$ as a function of μ for different values of L=1.

the non-trivial regime of the Kitaev chain.

In fact, by applying the lower-bound inequalities holding on SE [29, 35–37], it turns out that the constant value $E_{sq}^0 = \log(2)/2$ is a lower bound to the true SE $E_{sq}(\rho_{AB})$ between the edges at the exact topological point $\mu=0$. By continuity, the bound extends to neighboring values of μ . Since the upper bound $I_{(4)}$ and the lower bound E_{sq}^0 coincide in this region, both coincide with the true long-distance SE $E_{sq}(\rho_{AB})$ between edges A and B.

In conclusion, collecting all of the above results, the quantized TSE

$$E_{sq}(\rho_{AB}) = E_{sq}^0 = \frac{\log(2)}{2}$$
 (9)

is the order parameter for the Kitaev model of topological superconductivity.

The physical origin of a quantized non-vanishing longdistance entanglement between the system edges in the topological phase arises from the interplay between the exponential bulk-edge separation due to the topological nature of the system and the fundamental monogamy property of nonlocal quantum correlations [27].

As the two edges progressively decouple from the bulk their mutual information and correlation are enhanced by the monogamy constraint on the shared information and on the amount of shareable entanglement among the different subsystems. When the system moves away from the topological phase, correlations become once again short-ranged and the long-distance entanglement between the two extremes of the chain collapses.

The quantized limit of the edge–edge TSE is $\log(2)/2$ rather than the maximal Bell–pair entanglement $\log(2)$ because of the non-vanishing entanglement pattern existing between the internal degrees of freedom inside each edge.

B. SE and TSE: discriminating between symmetry breaking and topological order

A core question concerns the ability of a proposed order parameter to discriminate systems with topological order from systems with spontaneous symmetry breaking and Ginzburg-Landau type of order, addressing their different entanglement properties and patterns.

We focus our attention on the Ising spin-1/2 chain and the fermionic Kitaev chain. Setting $t=\Delta=1$ and applying the global Jordan-Wigner transformations [62], the Hamiltonian in Eq. (8) can be mapped into that of the 1D Ising model in transverse field:

$$H_I = J \sum_{j=1}^{L-1} \sigma_j^x \sigma_{j+1}^x + h \sum_{j=1}^{L} \sigma_j^z,$$
 (10)

with J=-2t and $h=\mu/2$. Both models share a twofold degenerate ground state and the parity symmetry \mathcal{Z}_2 , but the physics of the order displayed is radically different. While in the Ising model the \mathcal{Z}_2 spin reflection symmetry is spontaneously broken with the appearance of a nonvanishing local order parameter, the topological degeneracy in the Kitaev chain is realized with perfect conservation of the Hamiltonian symmetry and no local order parameters.

Despite the different type of order that they support, the two models share the same bipartite entanglement spectrum and bipartite von Neumann block entanglement entropy. This is not surprising, since the nonlocal Jordan-Wigner transformation (a particular case of the general Klein transformation in quantum field theory) does not affect the short-distance entanglement structure across the separation between the system's halves for Hamiltonians sums of local (nearest-neighbor or short-ranged) interaction terms.

The landscape is quite different when dealing with long-distance entanglement structures between the system's boundaries: clearly, they are expected to be significantly affected under the action of global transformations on the entire system.

In panels (a) and (b) of Fig. 4 we report the behavior of the end-to-end QCMI $I_{(3)}$ for the Ising and the Kitaev chains for two lengths L=6 and L=9. The two curves intersect at the critical points h=1 and $\mu=2$. In the thermodynamic limit, the following behaviors are expected: $I_{(3),Ising}/E^0_{sq,Ising}=1$ $(I_{(3),Kitaev}/E^0_{sq,Kitaev}=1)$ for 0< h<1 $(0<\mu<2)$ and $I_{(3),Ising}/E^0_{sq,Ising}=0$

 $(I_{(3),Kitaev}/E^0_{sq,Kitaev}=0)$ for h>1 $(\mu>2)$. This analysis shows that the QCMI $I_{(3)}$ detects and characterizes both topological and symmetry breaking orders but it is not capable of distinguishing between them.

In panels (c) and (d) of Fig. 4 we report the behavior of the end-to-end QCMI $I_{(4)}$ for the Ising and Kitaev chains; we see that $I_{(4)}$ distinguishes topological order from ordered phases with spontaneously broken symmetries.

For the Ising chain, we see that removing any finite part C_2 of the bulk $C=C_1C_2$ before performing the partial trace with respect to the reminder C_1 returns a strongly suppressed end-to-end QCMI $I_{(4)}$ that is expected to vanish in the thermodynamic limit.

At variance with the symmetry-breaking case, the topology of the Kitaev chain is essentially concentrated on the boundaries, so that in the computation of the end-to-end QCMIs performing the partial trace with respect to the entire bulk C is entirely equivalent to removing a part of the bulk (C_2) and then performing the partial trace with respect to the remaining part of the bulk (C_1) . As a consequence, $I_{(3)} = I_{(4)}$ for a topological system, while in general $I_{(3)} \neq I_{(4)}$ for a system with symmetry-breaking order.

Ultimately, these results depend on and highlight the different global properties of the two systems. Indeed, the bulk of the Kitaev chain is insulating and exponentially decoupled from the boundaries, forcing (by monogamy) the onset of the long-distance correlation between the ends of the chain.

Viceversa, the bulk of the Ising chain is conductive, so that cutting one part of it before performing the partial trace on the reminder abruptly interrupts the information flow and destroys the correlation structure between the two ends of the chain. These physical differences determine the different structure of the end-to-end QCMIs and of the end-to-end SE.

Concerning quadripartitions, an interesting, although not surprising, feature is the independence of the results on the relative sizes of the two parts of the bulk C_2 (the cut) and C_1 (the reminder), so that one can always adopt the most convenient choice $C_1 = 1$ in the actual calculations

In Fig. 5 panel (a) we report the behavior of the difference $I_{(4)}-E^0_{sq}$ as a function of L_{C_1} with $\mu=0.5,\,t=1$ and L=60, and for $\Delta=t$ (green curve) and $\Delta=0.1t$ (red curve). We see that $I_{(4)}-E^0_{sq}$ is constant in both cases, regardless of the length L_{C_1} .

In the balanced hopping-pairing case $t=\Delta$, the SE is fully quantized at the fundamental unit $E_{sq}^0=\log(2)/2$ already for an intermediate chain length of L=60 (green curve), while in the strongly unbalanced case $\Delta=0.1t$ one can observe (red curve) a small finite-size effect on $I_{(4)}-E_{sq}^0$.

These behaviors show that the balanced case $t=\Delta$

These behaviors show that the balanced case $t = \Delta$ is way more insensitive to finite size effects than the unbalanced case $t \neq \Delta$. On the other hand, as the inset in panel (a) of Fig. 5 shows, for the unbalanced case

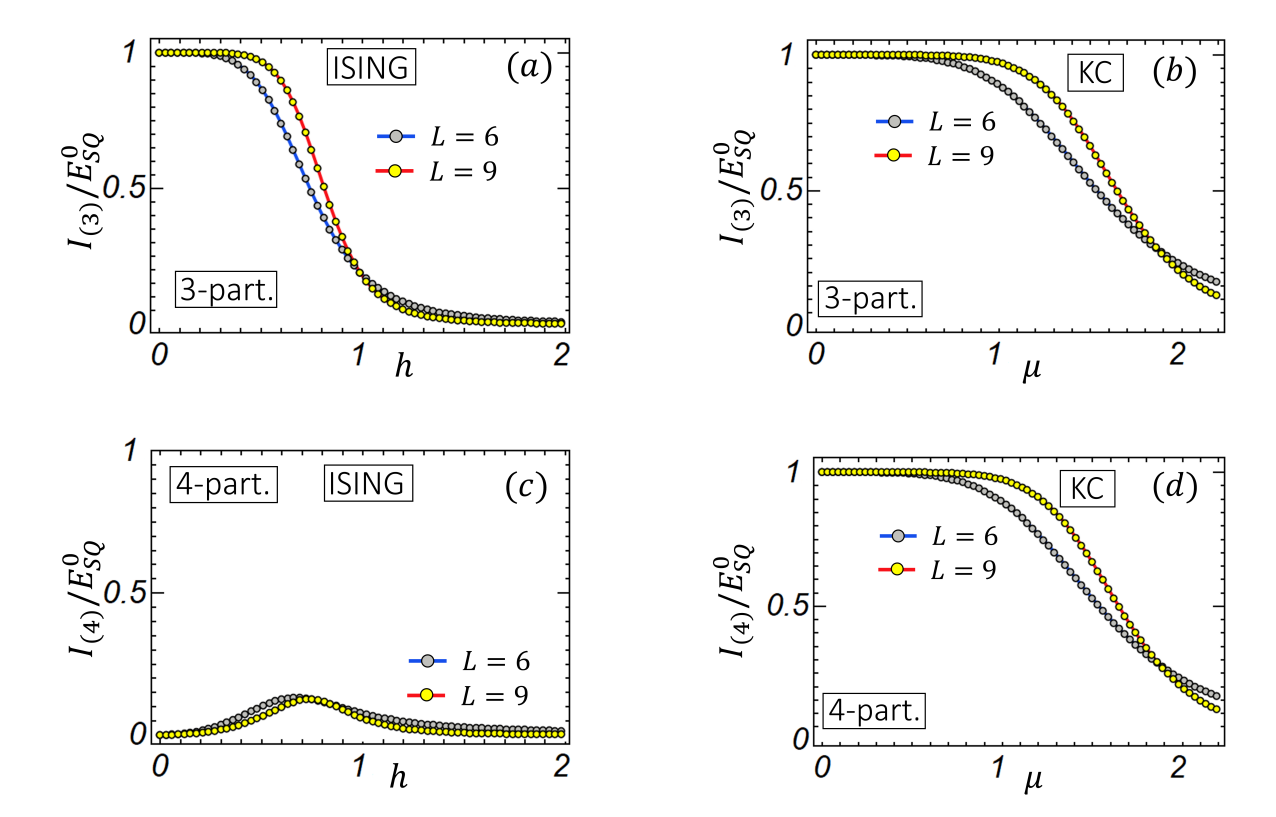


FIG. 4. Ratios of the end-to-end QCMIs $I_{(3)}$ and $I_{(4)}$ to the TSE $E_{SQ}^0 = \log(2)/2$ for the Ising chain (panels (a) and (c)) as functions of the transverse field h, and for the Kitaev chain (panels (b) and (d)) as functions of the chemical potential μ . While for the Kitaev chain the equality $I_{(3)} = I_{(4)}$ always holds, for the Ising chain $I_{(3)} \neq I_{(4)}$ and $I_{(4)}$ tends to vanish as the system size increases. The QCMI $I_{(4)}$ discriminates between topological and symmetry-breaking systems. Throughout, the Hamiltonian parameters are $t = \Delta = 1$ for the Kitaev chain and J = -1 for the Ising chain.

 $t \neq \Delta$ the difference $I_{(4)} - E_{sq}^0$ decreases with increasing system's sizes, tending to vanish, as expected, in the thermodynamic limit.

The different robustness to finite size effects between the balanced and unbalanced configurations is illustrated in panels (b) and (c) of Fig. 5, where we draw sketches of the Kitaev chain in the basis of Majorana fermions $a_j = c_j + c_j^{\dagger}$ and $b_j = -i(c_j - c_j^{\dagger})$ for the two aforementioned cases.

The balanced setting $t = \Delta$ illustrated in panel (c) results in turning off the coupling $(t - \Delta)$ $a_j b_{j+1}$ between third-neighboring Majorana fermions. In this configuration the Majorana fermions are thus more weakly coupled than in the unbalanced case $t \neq \Delta$ illustrated in panel (b).

On the other hand, the setting $t = \Delta$ and $\mu = 0$ corresponds to the exact analytic, topological degeneracy point of the model, where the edge modes a_1 and b_L decouple from the lattice and become exact zero energy modes.

C. TSE in the presence of interactions

The interacting Kitaev chain is obtained by adding a nearest-neighbor density-density interaction term to the free Kitaev Hamiltonian:

$$H_{IK} = H_K + U \sum_{j=1}^{L-1} n_j n_{j+1},$$
 (11)

where U is the interaction coupling constant and $n_j = c_j^{\dagger}c_j$ is the on site fermion number operator. The intervals U > 0 and U < 0 correspond, respectively, to a repulsive and to an attractive interaction. The phase diagram of the model has been investigated in depth by a variety of numerical and approximate analytical methods [58, 81, 83, 84] and is reported schematically in Fig. 6.

We see that, although very strong repulsive interactions eventually force the system into a Mott insulating phase, a topological superconducting state is established in between the trivial band insulator phase and the Mott localization even for fairly strong repulsive interactions. The black dashed line inside the topological phase is the factorization line of equation $\mu = \mu^*$ described in the following.

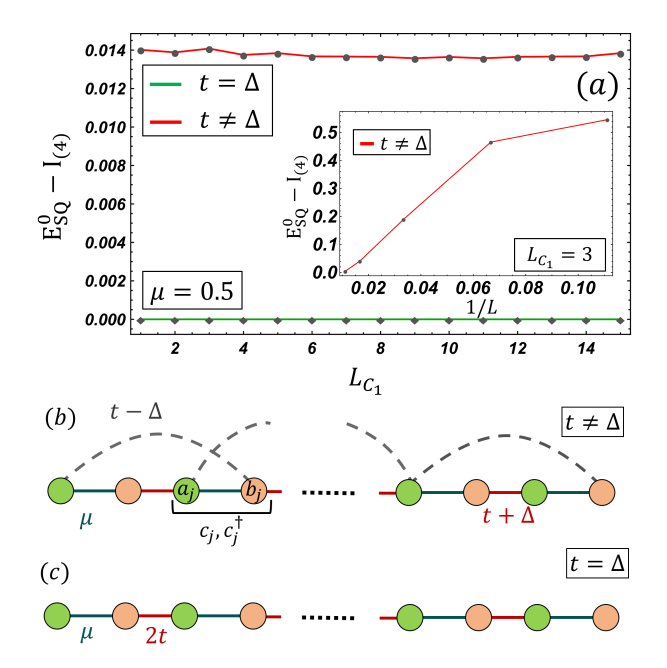


FIG. 5. Panel (a): Behavior of the QCMI $I_{(4)}$ as a function of the size L_{C_1} of the reminder of the bulk in a Kitaev chain of L=60 sites. We have considered both the balanced case $t=\Delta=1$ (green curve) and the unbalanced case t=1, $\Delta=0.1$ (red curve). Different choices of L_{C_1} have no effect on the evaluation of $I_{(4)}$. The inset shows the scaling of $I_{(4)}$ towards the quantized value $E_{SQ}^0 = \log(2)/2$ of the TSE in the balanced regime as the size L of the chain is increased. Panel (b): Schematic representation of the chain in the Majorana basis $\{a_i, b_i\}$ for $t \neq \Delta$. Panel (c): Same, with $t=\Delta$.

The interacting Kitaev chain can be mapped exactly onto the interacting XYZ spin-1/2 model in an external magnetic field

$$H_{xyz} = \sum_{j=1}^{L-1} \left[J_x \sigma_j^x \sigma_{j+1}^x + J_y \sigma_j^y \sigma_{j+1}^y + J_z \sigma_j^z \sigma_{j+1}^z \right] + h \sum_{j=1}^{L} \sigma_j^z,$$
(12)

where $J_x = -(\Delta + t)/2$, $J_y = (\Delta - t)/2$, $J_z = -U$, and $h = \mu/2$.

The model admits exact ground state solutions factorized in the product of single-spin (single-site) wave functions along the so-called factorization line $h=h^*=z_d\sqrt{(J_x+J_z)(J_y+J_z)}$ in any dimension [78, 79, 85], with z_d the coordination number (so that, e.g., $z_d=2$ in the 1D case).

For the Kitaev chain, this corresponds to the exact solution for the many-body ground states along the factorization line [81]:

$$\mu = \mu^* = 4\sqrt{U^2 + t \ U + (t^2 - \Delta^2)/4},$$
 (13)

which reduces to $\mu^* = 4\sqrt{U(U+t)}$ for $t = \Delta$.

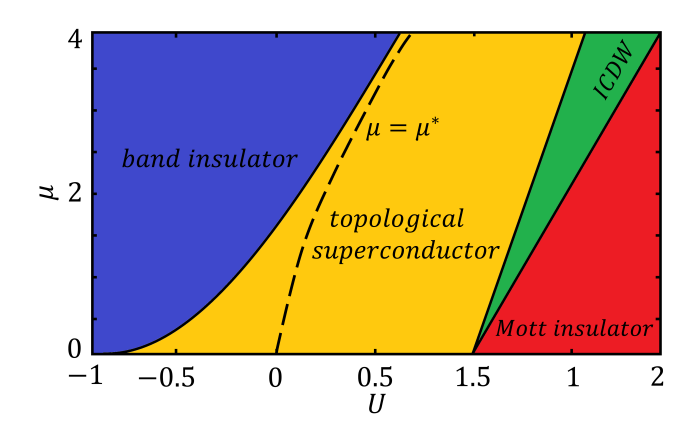


FIG. 6. Phase diagram of the interacting Kitaev chain on the μ -U plane for $\Delta=t$. The dashed black curve is the factorization line $\mu=\mu^*=4\sqrt{U^2+t\,U}$. It starts at the exact topological degeneracy point $\mu=U=0$, develops entirely inside the topological phase, and pinches asymptotically into the trivial phase for sufficiently large values of μ and U.

In general, along any factorization line (provided it exists) an interacting model Hamiltonian H becomes frustration–free and can be written as the sum of commuting local terms H_j : $H = \sum_j H_j$ with $[H_i, H_j] = 0$ [80].

The exact ground states of definite symmetry of the interacting Kitaev chain for $\mu = \mu^*$ are the following entangled linear combinations [81]:

$$|\Psi^{even}\rangle = \frac{1}{\sqrt{2}} (|\Psi^{+}\rangle + |\Psi^{-}\rangle)$$
 (14)

$$|\Psi^{odd}\rangle = \frac{1}{\sqrt{2}} (|\Psi^{+}\rangle - |\Psi^{-}\rangle),$$
 (15)

where the non-orthogonal states $|\Psi^{+}\rangle$ and $|\Psi^{-}\rangle$ are fully factorized in the product of single-site wave functions and read [81]:

$$|\Psi^{\pm}\rangle = \frac{1}{(\alpha+1)^{L/2}} e^{\pm \alpha c_1^{\dagger}} \dots e^{\pm \alpha c_L^{\dagger}} |vac\rangle, \quad (16)$$

where

$$\alpha = \sqrt{\cot(\theta^*/2)}, \quad \theta^* = \arctan(2\Delta/\mu^*),$$
 (17)

with $|vac\rangle$ denoting the lattice vacuum state.

The ground states $|\Psi^{even}\rangle$ and $|\Psi^{odd}\rangle$ are orthogonal and are the only possible ground state of H_{IK} for $\mu=\mu^*$. Ground state factorization holds in the topological phase with a repulsive interaction $U \geq 0$, and the even and odd ground states are degenerate with energy $E_0 = -(L-1)(U+t)$.

The behavior of the QCMI $I_{(4)}$ normalized to the quantized value of the SE $E_{sq}^0 = log(2)/2$ along the Illuminati-Katsura factorization line $\mu = \mu^*$ is reported in Fig. 7 panel (a) as a function of the chain length L for different values of the interaction strength, and in panel (b) as a

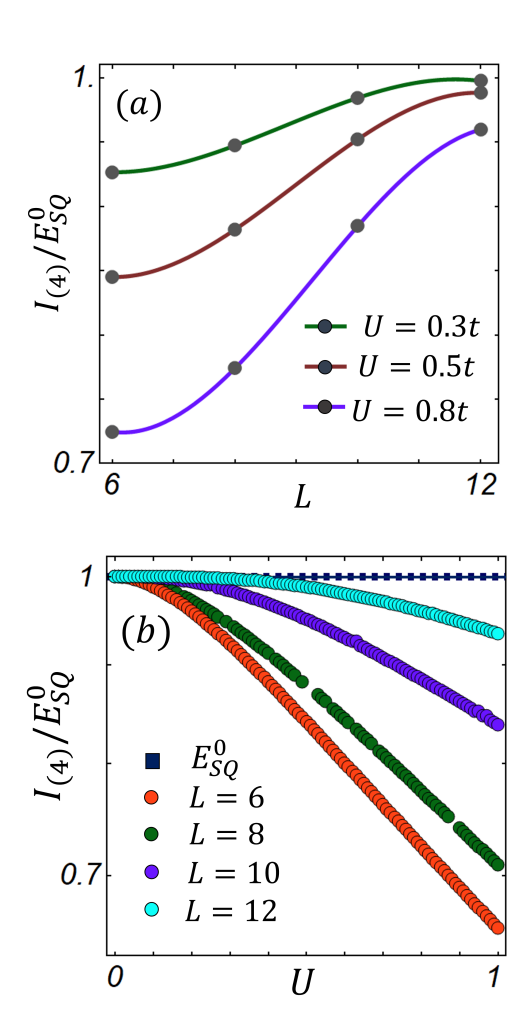


FIG. 7. The QCMI to TSE ratio $I_{(4)}/E_{sq}^0$ for the exact ground state solutions of the interacting Kitaev chain on the Illuminati-Katsura factorization line $\mu=\mu^*$ as a function of the chain length L for different values of the interaction strength U (panel (a)), and as a function of U for different values of L (panel (b)). In both cases the scaling behavior of $I_{(4)}$ converges to the quantized value log(2)/2 of the TSE for the non-interacting Kitaev chain. Eventually, for increasingly large values of U, the factorization line pinches into the trivial phase and the QCMI $I_{(4)}$ vanishes asymptotically. Throughout, $t=\Delta$ and $L_e=L/3$.

function of the interaction strength for different values of the chain length L.

The QCMI $I_{(4)}$ exhibits the correct scaling, saturating to the quantized value log(2)/2 of the SE for sufficiently large values of the chain size L, and vanishing asymptotically for very large values of the interaction strength U as the factorization line pinches the boundary of the topological phase and the system enters in the trivial phase.

In conclusion, we see that the TSE E_{sq}^0 identifies the correct quantized order parameter for the topological phase of the fermionic Kitaev chain, either free or interacting.

D. Robustness of TSE against disorder

Topological phases of the Kitaev chain are immune to the detrimental effects of disorder and local perturbations [52, 86–88]. Such immunity is a fundamental property that is expected to hold whenever topological order is involved. This observation suggests that $I_{(4)}$ should also be as immune to disorder as the other topological signatures previously defined in terms of the spectral properties [89] or related to the transport properties [90] of the systems involved.

We study two distinct classes of configurations, each characterized by a different source of disorder with a clear tracking of its physical origin. Since one of the way to realize a topological Kitaev chain is by proximity effect between a semiconducting nanowire and a conventional superconductor [39, 40], we consider two distinct sources of disorder: random site-dependent hopping amplitudes t_i and random site-dependent pairing potentials Δ_i . The former models an effective mass gradient and random doping along the nanowire, originating from the growth process of the nanowire itself, while the latter emulates unwanted spatial variations along the wire which can affect the nanowire-superconducting coupling and therefore the induced superconducting gap.

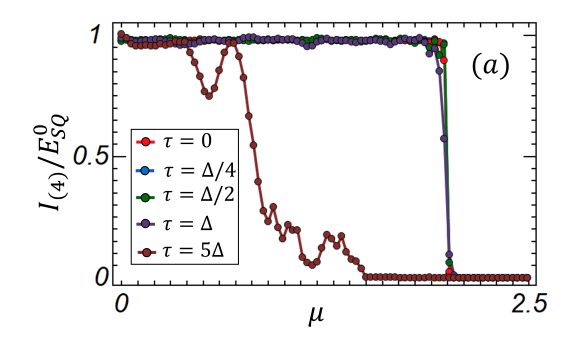
In Fig. 8 we report the behavior of the QCMI to TSE ratio $I_{(4)}/E_{sq}^0$ of the Kitaev chain Eq. 8 as a function of the chemical potential μ for the aforementioned two different sources of disorder. In panels (a) and (b) we consider respectively random hopping integrals $t_i = t + \tau_i^{dis}$ and random pairing potentials $\Delta_i = \Delta + \delta_i^{dis}$ with the random strengths of disorder τ_i^{dis} and δ_i^{dis} uniformly distributed in the intervals $(-\tau, \tau)$ and $(-\delta, \delta)$.

In Fig. 8, for the sake of completeness disorder effects are investigated spanning the spectrum of noise strengths from the perturbative regime up to the strongly disordered configurations. It is worth remarking that the maximum noise amplitudes considered correspond to extreme levels of disorder, which are not even expected in realistic experimental conditions.

Fig. 8 shows that within the typical regimes of weak to moderate disorder the TSE order parameter is strongly resilient up to the transition point, as it should be expected.

TSE and topological order are completely destroyed for very strong levels of noise on the hopping integrals (see panel (a)), while they are preserved in all regimes of disorder on the pairing amplitudes (see panel (b)), showing that noise on the hopping is more effective in perturbing the topological phase. In particular, in order to even allow a superconducting phase the maximum δ can never exceed Δ .

In conclusion, we have found that realistic values of the noise strengths do not perturb TSE significantly, thus indicating that the latter enjoys resilience against disorder, a crucially necessary feature of any candidate topological order parameter.



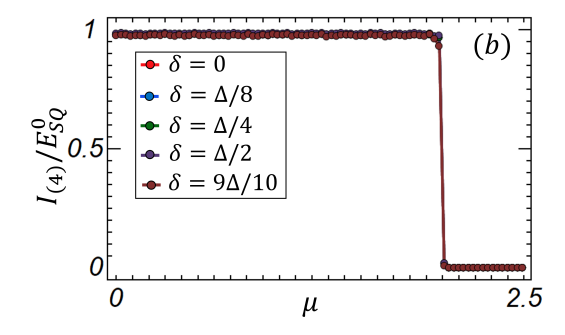


FIG. 8. The QCMI to TSE ratio $I_{(4)}/E_{sq}^0$ as a function of the chemical potential μ for a chain of length L=70 and two different types of disorder. Panel (a): behavior of $I_{(4)}/E_{sq}^0$ in the presence of random hopping amplitudes t_i . Panel (b): behavior of $I_{(4)}/E_{sq}^0$ in the presence of random pairing potentials Δ_i . The random realizations are generated by a continuous probability distribution defined in the interval $t_i \in (t-\tau, t+\tau)$, $\Delta_i \in (\Delta-\delta, \Delta+\delta)$. The reference values of the parameters have been fixed as t=1, $\Delta=0.1$. The different curves are parameterized by disorder of increasing strength.

V. SYSTEMS WITH MULTIPLE EDGE MODES: TSE OF THE KITAEV LADDER

In this section we generalize the previous investigations to consider systems enjoying multiple topological phases and multiple MZEMs, i.e. more than one Majoran zero mode per edge.

Various such generalizations of the 1D Kitaev model have been introduced [45–48, 91, 92], but the simplest instance can be realized by coupling multiple Kitaev chains with transverse hopping and pairing terms to form n-legs Kitaev ladders [49, 93]. The two-leg Kitaev ladder is the simplest model which takes into account multimode topological phases, which usually arise in models of significant complexity, often involving two-dimensional platforms [94–96].

The Hamiltonian H_{KL} of the two-leg Kitaev ladder can be expressed as follows:

$$H_{KL} = H_{K_1} + H_{K_2} + H_{K_{12}}, (18)$$

where H_{K_i} (j = 1, 2) is the Hamiltonian of a single

Kitaev chain and

$$H_{K_{12}} = \sum_{i=1}^{L} \left[-t_1 c_{i,1}^{\dagger} c_{i,2} + \Delta_1 c_{i,1} c_{i,2} + h.c. \right]$$
 (19)

describes the coupling between the two chains by means of a transverse hopping with amplitude t_1 and a transverse pairing with amplitude Δ_1 . The model has been introduced and discussed at length in Ref. [49]. The Kitaev ladder satisfies particle-hole, time reversal and chiral symmetry, belonging to the BDI class of the ten-fold classification.

The phase diagram of the model can be investigated by means of the winding number:

$$W = Tr \int_{-\pi}^{\pi} \frac{dk}{2\pi i} A_k^{-1} \partial_k A_k =$$

$$- \int_{-\pi}^{\pi} \frac{dk}{2\pi i} \partial_k \ln Det A_k$$
 (20)

where A_k can be expressed in terms of the model parameters once periodic boundary conditions have been imposed and the bulk-edge correspondence is invoked:

$$A_k = \begin{pmatrix} \epsilon_k - \Delta_k & -t_1 - \Delta_1 \\ -t_1 + \Delta_1 & \epsilon_k - \Delta_k \end{pmatrix}, \tag{21}$$

where $\epsilon_k = 2t \cos k + \mu$, $\Delta_k = 2i\Delta \sin k$ and $k \in [-\pi, \pi]$.

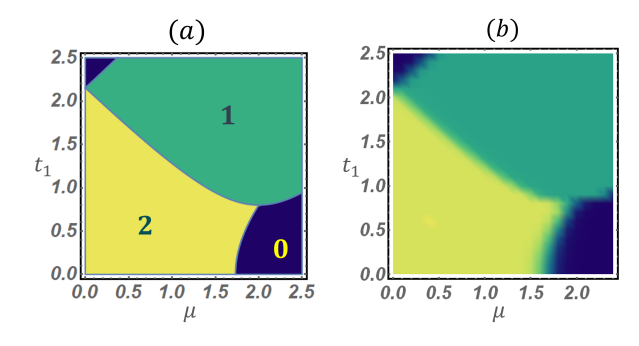
In panels (a), (c), and (b) of Fig. 9 we report the phase diagrams of the ladder obtained respectively by means of the winding number (panels (a) and (c)) and by means of the QCMI $I_{(4)}$ normalized by the quantized edge-edge TSE E_{sq}^0 (panel (b)). The diagram in panel (b) is obtained for a ladder of L=50 sites per chain, with $L_e=12$ and via interpolation on a grid of 25×25 points.

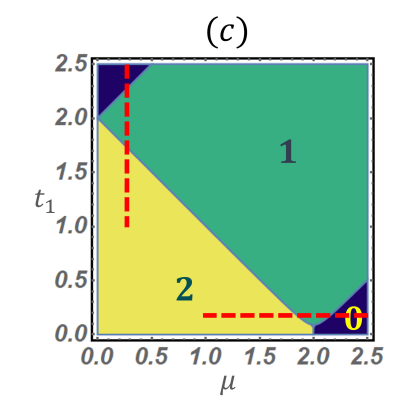
The digits drawn on the phase diagrams in panels (a) and (c) count the number of Majorana zero energy modes per ladder edge. Indeed, the system possesses a richer phase diagram compared to the one of the single Kitaev chain. Denoting by N_m the number of Majorana zero energy modes per edge, the two-leg Kitaev ladder features two alternating topological phases, respectively endowed with $N_m = 1$ and $N_m = 2$, and a trivial phase with no edge modes.

Despite the fact that the phase diagram in panels (a) and (c) is defined in terms of bulk properties, while the phase diagram in panel (b) is obtained in terms of the topological boundary entanglement, they show an excellent qualitative and quantitative agreement already at moderate system sizes.

In panel (c), we report the contour plot of the winding number for a different set of parameters, suitable to stand out transitions crossing all the three different phases 2-1-0, once either t_1 or μ have been fixed.

In panels (d) and (e) we report the behavior of $I_{(4)}/E_{sq}^0$ along the horizontal and vertical red cuts of panel (c). In both cases, we observe the three plateaux $I_{(4)}/E_{sq}^0$ =





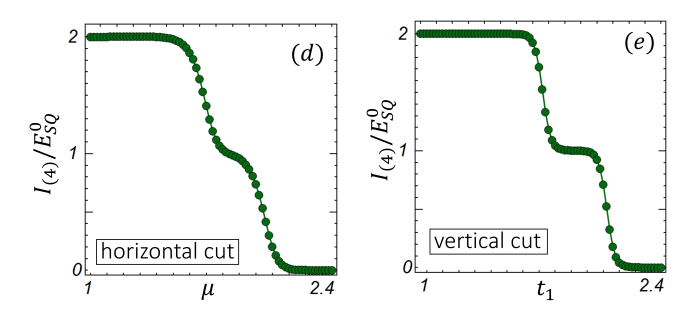


FIG. 9. Panels (a) and (c): phase diagram of the two-leg Kitaev ladder determined by means of the winding number in k-space. Panel (a): phase diagram with parameters fixed at t=1, $\Delta=0.8$, $\Delta_1=0.8$. Panel (c): phase diagram with parameters fixed at t=1, $\Delta=0.8$, $\Delta_1=0.09$. Panel (b): the same phase diagram determined by means of the QCMI to TSE ratio $I_{(4)}/E_{sq}^0$, obtained on a grid of 25×25 points with the order of the interpolating polynomial equal to 1. Panels (d) and (e): QCMI to TSE ratio $I_{(4)}/E_{sq}^0$, reported respectively along the horizontal and the vertical dashed red lines of panel (c). The single chain and edge lengths are fixed, respectively, at L=50 and $L_e=12$.

2,1,0 corresponding, respectively, to the two topological phases and to the trivial phase. Remarkably, TSE not only discriminates topological phases from trivial ones but also distinguishes different topological phases by counting the corresponding number of Majorana edge modes N_m :

$$\frac{I_{(4)}}{E_{sq}^0} = N_m \,. \tag{22}$$

If the above relation has general validity, then TSE can apply to systems belonging to arbitrary topological classes. Besides its conceptual importance, this property bears a clear practical advantage, since while the definition of the TSE is unique and system-independent, different invariants have to be defined each time, following the ten-fold classification, depending on the symmetries obeyed by each specific system under investigation.

VI. SYSTEMS WITH SUPPRESSED BULK EDGE CORRESPONDENCE: TSE OF THE KITAEV TIE

In this section we study by means of the TSE the effects of geometrical frustration induced by adding an hopping term of arbitrary spatial range to a Kitaev chain. The model has been introduced and investigated in Refs. [50, 64]. The tight-binding Hamiltonian of the model can be written as

$$H_T = H_K + H_d \,, \tag{23}$$

where H_K denotes the Kitaev chain Hamiltonian and

$$H_d = -t_d(c_d^{\dagger}c_{L-d+1} + h.c.)$$
 (24)

is an extra long-range hopping term, connecting two symmetrical sites of the chain d and L-d+1 with an hopping amplitude t_d . The long-range hopping, identified by the parameter d, can vary along the length of the chain, playing the role of a movable knot which induces a geometric frustration on the original chain Hamiltonian. This results in a legged-ring system with no clearly identifiable bulk, and consequently a suppressed bulk-edge correspondence, referred to as a Kitaev tie.

The phase diagram of the system in the μ -d plane shows an interstitial character with topological phases nucleating inside trivial regions as the knot position d is varied while keeping $\mu < 2t$. This phenomenon is referred to as topological frustration.

For small values of d, the interstitial character of the non-trivial phases is more evident, since the system resembles a ring with very short legs. On the other hand, for large values of d there is a significant growth of the topological phase domains, since the ring is reduced and the system approaches the limiting regime of a perturbed Kitaev chain.

The Kitaev tie is realizable in single-walled carbon nanotubes [50, 64], flexible ballistic conductors [97] where superconducting proximity effect can be easily implemented [98–100].

In Fig. 10, we report the behavior of the QCMI $I_{(4)}$ as a function of μ for a Kitaev tie of L=121 sites (blue curves) and we compare it with the behavior of the spectral energy function of the system (orange curves). Specifically, denoting by I_{max} the maximum value achieved by the QCMI $I_{(4)}$ and by E the lowest energy eigenvalue, in panel (a) we compare E and the

complement $1 - I_{(4)}/I_{max}$ of the QCMI normalized to its maximum value as functions of μ , while in panel (b) we compare E and the complement of the QCMI to TSE ratio $1 - I_{(4)}/E_{sq}^0$. We consider two different positions of the long-range hopping, respectively d = 30 (panel (a)) and d = 50 (panel (b)).

The presence of unpaired Majorana modes is related, respectively, to minima or vanishing values of the energy eigenvalue and to the minima of the TSE-related estimators. All plots clearly show signatures of the topological frustration, pinpointed by an oscillating behavior of the various quantities as functions of the chemical potential. For systems with an associated bulk, the QCMI $I_{(4)}$ converges to the quantized TSE E_{sq}^0 already for moderate lattice sizes, as shown in the discussion of the Kitaev chain and of the Kitaev ladder. For the Kitaev tie, the absence of an associated bulk is signaled by the fact that the complement of the QCMI to TSE ratio does not vanish, reaching instead non-zero minima, even for lattices of relatively large sizes (L=121).

On the other hand, the perfect correspondence of the positions of both the minima and the maxima of the different functions shows that the TSE captures the same physics as the energy. Although the energy eigenvalue provides a stronger marker of the presence of MZEMs, remarkably the QCMI $I_{(4)}$ and the TSE E^0_{sq} are reliable quantifiers of the emerging topological features even for systems, like the Kitaev tie, that do not allow for a clear identification of the bulk geometry.

Fig. 10 shows that the actual value of the absolute maximum I_{max} reached by the QCMI $I_{(4)}$ strongly depends on whether the scope d of the long-range hopping falls inside the edge extension, i.e. $d < L_e$, as in panel (a), or outside the edge extension, i.e. $d > L_e$, as in panel (b). Interestingly, $I_{(4)}$ exceeds E_{sq}^0 ($I_{max} \approx 0.62$) when $d < L_e$, while when $d > L_e$, the QCMI converges to the TSE E_{sq}^0 as in the cases of the Kitaev chains and ladders. In the case of the Kitaev tie the inapplicability of the bulk-edge correspondence is responsible for the partial loss of quantization of the QCMI.

VII. DISCUSSION AND OUTLOOK

In the present work we have discussed the application of squashed entanglement to the study of topological quantum matter. Squashed entanglement is a measure of bipartite entanglement defined on multipartitions that generalizes the von Neumann entanglement entropy; it allows to quantify the bipartite entanglement between any two subsystems in any quantum state, either pure or mixed, and reduces to the von Neumann entanglement entropy on pure states. Introducing generic tripartitions and quadripartitions of a quantum system, we have identified two general classes of upper bounds on the bipartite squashed entanglement in terms of quantum conditional mutual information between subsystems.

For models of topological superconductors that ad-

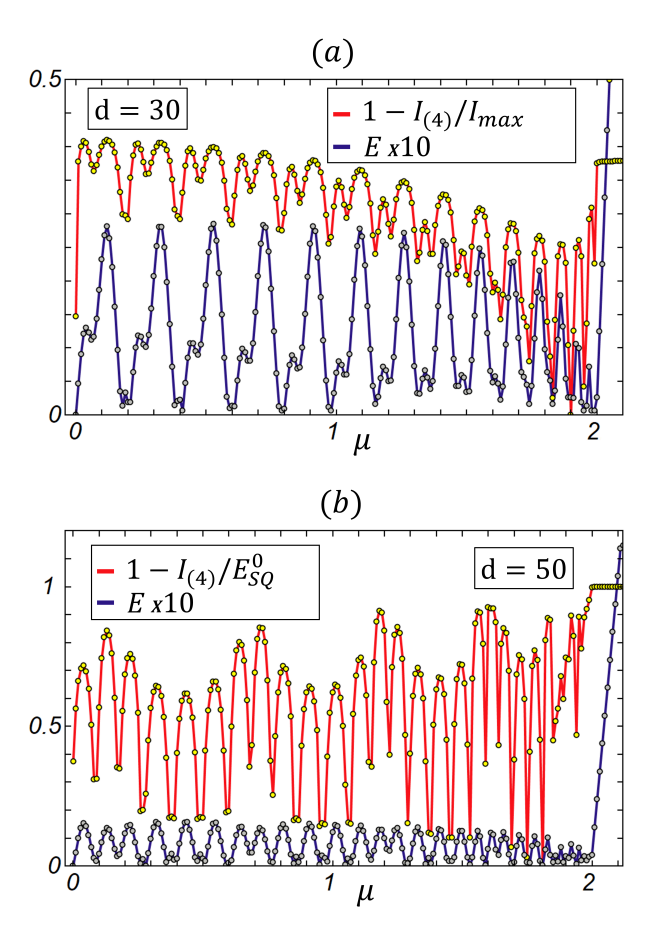


FIG. 10. Panel (a): Behavior of $1-I_{(4)}/I_{max}$ (red curve) and of the lowest energy eigenvalue E (blue curve) as functions of the chemical potential μ for a Kitaev tie of L=121 sites with d=30. Panel (b): behavior of $1-I_{(4)}/E_{sq}^0$ (red curve) and of E (blue curve) as functions of μ for the same Kitaev tie with d=50. The QCMI $I_{(4)}$ is evaluated for an edge length $L_e=40$. In all plots the Hamiltonian parameters are fixed at $t=t_d=1$ and $\Delta=0.02$.

mit Majorana zero energy modes at the system edges, we have shown that in the topological phase the upper bound associated to the system quadripartition in fact coincides with the squashed entanglement between the system edges in the ground state at the exact topological point. The squashed entanglement in the topological phase is quantized to $\log(2)/2$, half the value of the maximal Bell entanglement, counting the Majorana splitting of the Dirac fermions.

The long-distance topological squashed entanglement between the edges is constant throughout the topological phase, exhibits the correct scaling when approaching the critical point, and vanishes identically in the trivial phase. Moreover, it is robust in the presence of interactions, resilient to the effects of disorder and local perturbations, and discriminates topological order from orders associated to spontaneous symmetry breaking. It thus realizes the desired, and long-sought for, entanglement-based order parameter for symmetry-protected topologi-

cal superconductivity.

For systems with geometries of higher complexity with respect to the 1D Kitaev chain, featuring multiple topological phases and more than one Majorana zero energy mode per edge, like e.g. the Kitaev ladder, topological squashed entanglement distinguishes between the multiple phases by plateaux that count the number of Majorana edge modes. For systems with weakened bulkedge correspondence, like e.g. the Kitaev tie, topological squashed entanglement, though ceasing to be perfectly quantized, is anyway able to identify the interstitial topological phases and discriminate them from the trivial ones.

Given that on pure quantum states, e.g. ground states of many–body systems, the squashed entanglement reduces exactly to the von Neumann block entanglement entropy defined on bipartitions of a quantum system into two blocks, the subleading contribution to the block entropy, the block topological squashed entanglement, trivially coincides with the topological entanglement entropy in the case of true topological order in two-dimensional systems. Therefore squashed entanglement provides the general framework that unifies all classes of topological order in any dimension.

Concerning the experimental accessibility of topological squashed entanglement, the problem boils down to that of measuring quantum entropies of a set of reduced states in quantum many—body systems. A recent proposal relies on the thermodynamic study of the entanglement Hamiltonian for the direct experimental probing of von Neumann entropies via quantum quenches [101]. Another possibility, specific for systems featuring topological order, consists in identifying minimum entropy states and then experimentally simulating the behavior of the associated von Neumann entropies via the classical microwave analogs of such states. In this way it is in principle possible to simulate various non-trivial instances of reduced entropies and topological order, as shown explicitly for the transition from a trivial phase to a \mathcal{Z}_2 -

symmetric topological phase [102]. Since highly informative bounds on von Neumann entropies, quantum conditional mutual information, and squashed entanglement can be constructed in terms of Rényi entropies [36, 37], a further possibility is to adapt to fermionic systems [103] the schemes previously proposed for the experimental measurement of Rènyi entropies in bosonic and spin systems [104–106] and the corresponding experimental techniques that lead to the first experimental measurement of the 2-Rényi entropy in a many-body system [107].

The generality of the concept of squashed entanglement between subsystems on multipartitions allows for several possible future research directions. of investigation of current interest is the application of squashed entanglement to the study of topological quantum matter at finite temperature and out of equilibrium [108]. In fact, even for non topological matter it would be interesting to study finite temperature quantum criticality resorting to squashed entanglement and compare it systematically with other measures of nonclassicality such as, e.g., the entropic discord [109] or Bell nonlocality [110]. In this perspective, hierarchies of quantum complexity according to different layers of quantumness, ranging from discord and coherence to entanglement and nonlocality, could realize the scaffold of a unified research framework applicable to a wide spectrum of problems, ranging from quantum information and quantum matter to elementary particle physics and quantum gravity.

Acknowledgments – We acknowledge support by MUR (Ministero dell'Università e della Ricerca) via the project PRIN 2017 "Taming complexity via QUantum Strategies: a Hybrid Integrated Photonic approach" (QUSHIP) Id. 2017SRNBRK.

Author contributions – F.I. conceived the fundamental idea, organized the project and supervised the work. F. I. and A. Marino performed part of the calculations, while A. Maiellaro performed the full calculations and realized the figures. F. I. and A. Maiellaro drafted the manuscript, discussed the results and edited the paper.

B. Zeng, X. Chen, D.-L. Zhou, and X.-G. Wen, Quantum Information Meets Quantum Matter (Springer International Publishing, 2019).

^[2] N. Laflorencie, Quantum entanglement in condensed matter systems, Physics Reports 646, 1 (2016).

^[3] L. Carr, Understanding Quantum Phase Transitions (CRC Press, 2010).

^[4] J. Eisert, M. Cramer, and M. B. Plenio, Area laws for the entanglement entropy, Reviews of Modern Physics 82, 277 (2010).

^[5] L. Amico, R. Fazio, A. Osterloh, and V. Vedral, Entanglement in many-body systems, Rev. Mod. Phys. 80, 517 (2008).

^[6] S. Girvin and K. Yang, Modern Condensed Matter Physics (Cambridge University Press, 2019).

^[7] T. Ozawa and H. M. Price, Topological quantum matter in synthetic dimensions, Nature Reviews Physics 1, 349

^{(2019).}

^[8] C.-K. Chiu, J. C. Teo, A. P. Schnyder, and S. Ryu, Classification of topological quantum matter with symmetries, Reviews of Modern Physics 88, 035005 (2016).

^[9] X.-L. Qi and S.-C. Zhang, Area laws for the entanglement entropy, Reviews of Modern Physics 83, 1057 (2011).

^[10] M. Sato and Y. Ando, Topological superconductors: a review, Reports on Progress in Physics 80, 076501 (2017).

^[11] J. K. Pachos, Introduction to Topological Quantum Computation (Cambridge University Press, 2012).

^[12] J. Alicea, New directions in the pursuit of Majorana fermions in solid state systems, Reports on Progress in Physics 75, 076501 (2012).

^[13] C. Beenakker, Search for Majorana fermions in superconductors, Annual Review of Condensed Matter

- Physics 4, 113 (2013).
- [14] A. Hamma, R. Ionicioiu, and P. Zanardi, Ground state entanglement and geometric entropy in the Kitaev model, Physics Letters A 337, 22 (2005).
- [15] A. Kitaev and J. Preskill, Topological entanglement entropy, Physical Review Letters 96, 110404 (2006).
- [16] M. Levin and X.-G. Wen, Topological entanglement entropy, Physical Review Letters 96, 110405 (2006).
- [17] F. Pollmann, A. M. Turner, E. Berg, and M. Oshikawa, Entanglement spectrum of a topological phase in one dimension, Physical Review B 81, 064439 (2010).
- [18] R. Horodecki, P. Horodecki, M. Horodecki, and K. Horodecki, Quantum entanglement, Reviews of Modern Physics 81, 865 (2009).
- [19] I. Bengtsson and K. Życzkowski, Geometry of Quantum States: An Introduction to Quantum Entanglement (Cambridge University Press, 2020).
- [20] R. R. Tucci, Entanglement of distillation and conditional mutual information, arXiv:quant-ph/0202144 (2002).
- [21] M. Christandl and A. Winter, "squashed entanglement": An additive entanglement measure, Journal of Mathematical Physics 45, 829 (2004).
- [22] N. J. Cerf and C. Adami, Negative entropy and information in quantum mechanics, Physical Review Letters 79, 5194 (1997).
- [23] N. J. Cerf and C. Adami, Information theory of quantum entanglement and measurement, Physica D: Non-linear Phenomena 120, 62 (1998).
- [24] M. M. Wilde, Squashed entanglement and approximate private states, Quantum Information Processing 15, 4563 (2016).
- [25] R. Alicki and M. Fannes, Continuity of quantum conditional information, Journal of Physics A: Mathematical and General 37, L55 (2004).
- [26] F. G. S. L. Brandão, M. Christandl, and J. Yard, Faithful squashed entanglement, Communications in Mathematical Physics 306, 805 (2011).
- [27] M. Koashi and A. Winter, Monogamy of quantum entanglement and other correlations, Physical Review A 69, 022309 (2004).
- [28] I. Devetak and J. Yard, Exact cost of redistributing multipartite quantum states, Physical Review Letters 100, 230501 (2008).
- [29] K. Li and A. Winter, Relative entropy and squashed entanglement, Communications in Mathematical Physics **326**, 63 (2014).
- [30] D. Yang, K. Horodecki, M. Horodecki, P. Horodecki, J. Oppenheim, and W. Song, Squashed entanglement for multipartite states and entanglement measures based on the mixed convex roof, IEEE Transactions on Information Theory 55, 3375 (2009).
- [31] M. Takeoka, G. Saikat, and M. M. Wilde, The squashed entanglement of a quantum channel, IEEE Transactions on Information Theory 60, 4987 (2014).
- [32] Y. Huang, Computing quantum discord is np-complete, New Journal of Physics 16, 033027 (2014).
- [33] M. Christandl and A. Winter, Uncertainty, monogamy, and locking of quantum correlations, IEEE Transactions on Information Theory 51, 3159 (2005).
- [34] G. De Palma, The squashed entanglement of the noiseless quantum gaussian attenuator and amplifier, Journal of Mathematical Physics **60**, 112201 (2019).

- [35] E. A. Carlen and E. H. Lieb, Bounds for entanglement via an extension of strong subadditivity of entropy, Letters in Mathematical Physics 101, 1 (2012).
- [36] F. G. S. L. Brandão, A. W. Harrow, J. Oppenheim, and S. Strelchuk, Quantum conditional mutual information, reconstructed states, and state redistribution, Physical Review Letters 115, 050501 (2015).
- [37] O. Fawzi and R. Renner, Quantum conditional mutual information and approximate markov chains, Communications in Mathematical Physics 340, 575 (2015).
- [38] A. Y. Kitaev, Unpaired majorana fermions in quantum wires, Physics-Uspekhi 44, 131 (2001).
- [39] R. M. Lutchyn, J. D. Sau, and S. Das Sarma, Majorana fermions and a topological phase transition in semiconductor-superconductor heterostructures, Physical Review Letters 105, 077001 (2010).
- [40] Y. Oreg, G. Refael, and F. von Oppen, Helical liquids and majorana bound states in quantum wires, Physical Review Letters 105, 177002 (2010).
- [41] S. Nadj-Perge, I. K. Drozdov, B. A. Bernevig, and A. Yazdani, Proposal for realizing majorana fermions in chains of magnetic atoms on a superconductor, Physical Review B 88, 020407 (2013).
- [42] R. M. Lutchyn, E. P. A. M. Bakkers, L. P. Kouwenhoven, P. Krogstrup, C. M. Marcus, and Y. Oreg, Majorana zero modes in superconductor–semiconductor heterostructures, Nature Reviews Materials 3, 52 (2018).
- [43] V. Mourik, K. Zuo, S. M. Frolov, S. R. Plissard, E. P. A. M. Bakkers, and L. P. Kouwenhoven, Signatures of majorana fermions in hybrid superconductorsemiconductor nanowire devices, Science 336, 1003 (2012).
- [44] S. Nadj-Perge, I. K. Drozdov, J. Li, H. Chen, S. Jeon, J. Seo, A. H. MacDonald, B. A. Bernevig, and A. Yazdani, Observation of majorana fermions in ferromagnetic atomic chains on a superconductor, Science 346, 602 (2014).
- [45] A. C. Potter and P. A. Lee, Multichannel generalization of kitaev's majorana end states and a practical route to realize them in thin films, Physical Review Letters 105, 227003 (2010).
- [46] B. Zhou and S.-Q. Shen, Crossover from majorana edgeto end-states in quasi-one-dimensional p-wave superconductors, Physical Review B 84, 054532 (2011).
- [47] R. Wakatsuki, M. Ezawa, and N. Nagaosa, Majorana fermions and multiple topological phase transition in kitaev ladder topological superconductors, Physical Review B 89, 174514 (2014).
- [48] C. Schrade, M. Thakurathi, C. Reeg, S. Hoffman, J. Klinovaja, and D. Loss, Low-field topological threshold in majorana double nanowires, Physical Review B 96, 035306 (2017).
- [49] A. Maiellaro, F. Romeo, and R. Citro, Topological phase diagram of a kitaev ladder, The European Physical Journal Special Topics 227, 1397 (2018).
- [50] A. Maiellaro, F. Romeo, and R. Citro, Topological phases of a kitaev tie, The European Physical Journal Special Topics 229, 637 (2020).
- [51] J. Shapiro, The bulk-edge correspondence in three simple cases, Reviews in Mathematical Physics 32, 2030003 (2020).
- [52] S. S. Hegde and S. Vishveshwara, Majorana wavefunction oscillations, fermion parity switches, and disorder in kitaev chains, Physical Review B 94, 115166

- (2016).
- [53] H. Katsura and T. Koma, The noncommutative index theorem and the periodic table for disordered topological insulators and superconductors, Journal of Mathematical Physics 59, 031903 (2018).
- [54] W. DeGottardi, D. Sen, and S. Vishveshwara, Topological phases, majorana modes and quench dynamics in a spin ladder system, New Journal of Physics 13, 065028 (2011).
- [55] T. Zhan, X. Shi, Y. Dai, X. Liu, and J. Zi, Transfer matrix method for optics in graphene layers, Journal of Physics: Condensed Matter 25, 215301 (2013).
- [56] L. Fidkowski, Entanglement spectrum of topological insulators and superconductors, Physical Review Letters 104, 130502 (2010).
- [57] A. M. Turner, F. Pollmann, and E. Berg, Topological phases of one-dimensional fermions: An entanglement point of view, Physical Review B 83, 075102 (2011).
- [58] P. Fromholz, G. Magnifico, V. Vitale, T. Mendes-Santos, and M. Dalmonte, Entanglement topological invariants for one-dimensional topological superconductors, Physical Review B 101, 085136 (2020).
- [59] C. V. Kraus, M. Dalmonte, M. A. Baranov, A. M. Läuchli, and P. Zoller, Majorana edge states in atomic wires coupled by pair hopping, Physical Review Letters 111, 173004 (2013).
- [60] E. Wybo, F. Pollmann, S. L. Sondhi, and Y. You, Visualizing quasiparticles from quantum entanglement for general one-dimensional phases, Physical Review B 103, 115120 (2021).
- [61] E. M. Stoudenmire, J. Alicea, O. A. Starykh, and M. P. Fisher, Interaction effects in topological superconducting wires supporting Majorana fermions, Physical Review B 84, 014503 (2011).
- [62] F. Franchini, An Introduction to Integrable Techniques for One-Dimensional Quantum Systems (Springer International Publishing, 2017).
- [63] J. C. Budich and E. Ardonne, Equivalent topological invariants for one-dimensional majorana wires in symmetry class d, Physical Review B 88, 075419 (2013).
- [64] A. Maiellaro, F. Romeo, and R. Citro, Effects of geometric frustration in kitaev chains, The European Physical Journal Plus 136, 627 (2021).
- [65] L. Campos Venuti, S. M. Giampaolo, F. Illuminati, and P. Zanardi, Long-distance entanglement and quantum teleportation in xx spin chains, Physical Review A 76, 052328 (2007).
- [66] S. M. Giampaolo and F. Illuminati, Long-distance entanglement in many-body atomic and optical systems, New Journal of Physics 12, 025019 (2010).
- [67] S. M. Giampaolo, B. C. Hiesmayr, and F. Illuminati, Global-to-local incompatibility, monogamy of entanglement, and ground-state dimerization: Theory and observability of quantum frustration in systems with competing interactions, Physical Review B 92, 144406 (2015).
- [68] G. Gualdi, S. M. Giampaolo, and F. Illuminati, Modular entanglement, Physical Review Letters 106, 050501 (2011).
- [69] S. Zippilli, S. M. Giampaolo, and F. Illuminati, Surface entanglement in quantum spin networks, Physical Review A 87, 042304 (2013).
- [70] I. Peschel and V. Eisler, Reduced density matrices and entanglement entropy in free lattice models, Journal of

- Physics A: Mathematical and Theoretical **42**, 504003 (2009).
- [71] V. Eisler and I. Peschel, Properties of the entanglement hamiltonian for finite free-fermion chains, Journal of Statistical Mechanics: Theory and Experiment 2018, 104001 (2018).
- [72] M.-C. Chung and I. Peschel, Density-matrix spectra for two-dimensional quantum systems, Phys. Rev. B 62, 4191 (2000).
- [73] F. Parisen Toldin and F. F. Assaad, Entanglement hamiltonian of interacting fermionic models, Phys. Rev. Lett. 121, 200602 (2018).
- [74] M.-C. Chung and I. Peschel, Density-matrix spectra of solvable fermionic systems, Physical Review B 64, 064412 (2001).
- [75] J. Langbehn, Y. Peng, L. Trifunovic, F. von Oppen, and P. W. Brouwer, Reflection-symmetric second-order topological insulators and superconductors, Physical Review Letters 119, 246401 (2017).
- [76] R. Orús, A practical introduction to tensor networks: Matrix product states and projected entangled pair states, Annals of Physics 349, 117 (2014).
- [77] U. Schollwöck, The density-matrix renormalization group in the age of matrix product states, Annals of Physics 326, 96 (2011), january 2011 Special Issue.
- [78] S. M. Giampaolo, G. Adesso, and F. Illuminati, Theory of ground state factorization in quantum cooperative systems, Physical Review Letters 100, 197201 (2008).
- [79] S. M. Giampaolo, G. Adesso, and F. Illuminati, Separability and ground–state factorization in quantum spin systems, Physical Review B 79, 224434 (2009).
- [80] S. M. Giampaolo, G. Adesso, and F. Illuminati, Probing quantum frustrated systems via factorization of the ground state, Physical Review Letters 104, 207202 (2010).
- [81] H. Katsura, D. Schuricht, and M. Takahashi, Exact ground states and topological order in interacting kitaev/majorana chains, Physical Review B 92, 115137 (2015).
- [82] A. Altland and M. R. Zirnbauer, Nonstandard symmetry classes in mesoscopic normal-superconducting hybrid structures, Physical Review B 55, 1142 (1997).
- [83] F. Hassler and D. Schuricht, Strongly interacting majorana modes in an array of josephson junctions, New Journal of Physics 14, 125018 (2012).
- [84] E. Sela, A. Altland, and A. Rosch, Majorana fermions in strongly interacting helical liquids, Physical Review B 84, 085114 (2011).
- [85] S. M. Giampaolo, S. Montangero, F. Dell'Anno, S. De Siena, and F. Illuminati, Universal aspects in the behavior of the entanglement spectrum in one dimension: Scaling transition at the factorization point and ordered entangled structures, Physical Review B 88, 125142 (2013).
- [86] P. W. Brouwer, M. Duckheim, A. Romito, and F. von Oppen, Probability distribution of majorana end-state energies in disordered wires, Physical Review Letters 107, 196804 (2011).
- [87] P. Neven, D. Bagrets, and A. Altland, Quasiclassical theory of disordered multi-channel majorana quantum wires, New Journal of Physics 15, 055019 (2013).
- [88] I. Adagideli, M. Wimmer, and A. Teker, Effects of electron scattering on the topological properties of nanowires: Majorana fermions from disorder and su-

- perlattices, Physical Review B 89, 144506 (2014).
- [89] D. Sticlet, C. Bena, and P. Simon, Spin and majorana polarization in topological superconducting wires, Physical Review Letters 108, 096802 (2012).
- [90] C. W. J. Beenakker, Random-matrix theory of quantum transport, Reviews of Modern Physics 69, 731 (1997).
- [91] M. Wimmer, A. R. Akhmerov, M. V. Medvedyeva, J. Tworzydło, and C. W. J. Beenakker, Majorana bound states without vortices in topological superconductors with electrostatic defects, Physical Review Letters 105, 046803 (2010).
- [92] B.-Z. Zhou, D.-H. Xu, and B. Zhou, Majorana zero modes in a ladder of density-modulated kitaev superconductor chains, Physics Letters A 381, 2426 (2017).
- [93] A. Maiellaro, F. Romeo, C. A. Perroni, V. Cataudella, and R. Citro, Unveiling signatures of topological phases in open kitaev chains and ladders, Nanomaterials 9, 10.3390/nano9060894 (2019).
- [94] W. A. Benalcazar, B. A. Bernevig, and T. L. Hughes, Quantized electric multipole insulators, Science 357, 61 (2017).
- [95] X.-W. Xu, Y.-Z. Li, Z.-F. Liu, and A.-X. Chen, General bounded corner states in the two-dimensional suschrieffer-heeger model with intracellular next-nearest-neighbor hopping, Physical Review A 101, 063839 (2020).
- [96] A. Maiellaro and R. Citro, Topological edge states of a majorana bbh model, Condensed Matter 6 (2021).
- [97] G. Refael, J. Heo, and M. Bockrath, Sagnac interference in carbon nanotube loops, Physical Review Letters 98, 246803 (2007).
- [98] A. Kasumov, R. Deblock, M. Kociak, B. Reulet, H. Bouchiat, I. Khodos, Y. Gorbatov, V. Volkov, C. Journet, O. Stephan, and M. Burghard, Proximityinduced superconductivity in carbon nanotubes, Comptes Rendus de l'Académie des Sciences - Series IIB - Mechanics-Physics-Astronomy 327, 933 (1999).
- [99] M. Marganska, L. Milz, W. Izumida, C. Strunk, and M. Grifoni, Majorana quasiparticles in semiconducting carbon nanotubes, Physical Review B 97, 075141

- (2018).
- [100] L. Milz, W. Izumida, M. Grifoni, and M. Marganska, Transverse profile and three-dimensional spin canting of a majorana state in carbon nanotubes, Physical Review B 100, 155417 (2019).
- [101] T. Mendes-Santos, G. Giudici, R. Fazio, and M. Dalmonte, Measuring von neumann entanglement entropies without wave functions, New Journal of Physics 22, 013044 (2020).
- [102] T. Chen, S. Zhang, and et al., Experimental observation of classical analogy of topological entanglement entropy, Nature Communications 10, 1557 (2019).
- [103] E. Cornfeld, E. Sela, and M. Goldstein, Measuring fermionic entanglement: Entropy, negativity, and spin structure, Physical Review A 99, 062309 (2019).
- [104] D. A. Abanin and E. Demler, Measuring entanglement entropy of a generic many-body system with a quantum switch, Physical Review Letters 109, 020504 (2012).
- [105] A. J. Daley, H. Pichler, J. Schachenmayer, and P. Zoller, Measuring entanglement growth in quench dynamics of bosons in an optical lattice, Physical Review Letters 109, 020505 (2012).
- [106] A. Elben, B. Vermersch, M. Dalmonte, J. I. Cirac, and P. Zoller, Rényi entropies from random quenches in atomic hubbard and spin models, Physical Review Letters 120, 050406 (2018).
- [107] R. Islam, R. Ma, P. M. Preiss, M. E. Tai, A. Lukin, M. Rispoli, and M. Greiner, Measuring entanglement entropy in a quantum many-body system, Nature 528, 77 (2015).
- [108] M. McGinley and N. R. Cooper, Interacting symmetryprotected topological phases out of equilibrium, Physical Review Research 1, 033204 (2019).
- [109] P. S. Tarabunga, T. Mendes-Santos, F. Illuminati, and M. Dalmonte, Finite-temperature quantum discordant criticality, arXiv:2110.10597 (2021).
- [110] W. Roga, A. Maiellaro, L. Petruzziello, M. Takeoka, and F. Illuminati, Resource theory of quantum nonlocality: Geometric bell nonlocality in hilbert space, In preparation (2022).